Inorganic Chemistry

pubs.acs.org/IC

Article

Formation of Iridium(III) and Rhodium(III) Amine, Imine, and Amido Complexes Based on Pyridine−Amine Ligands: Structural Diversity Arising from Reaction Conditions, Substituent Variation, and Metal Centers

Xueyan Hu, Lihua Guo,* Mengqi Liu, Mengru Sun, Qiuya Zhang, Hongwei Peng, Fanjun Zhang, and Zhe Liu*

Cite This: *Inorg. Chem.* 2022, 61, 10051−10065

Read Online

ACCESS | Metrics & More | Article Recommendations | Supporting Information

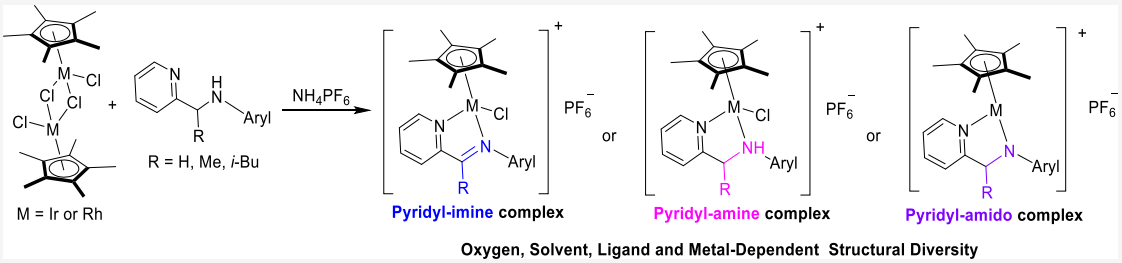

ABSTRACT: Herein, we present the different coordination modes of half-sandwich iridium(III) and rhodium(III) complexes based on pyridine−amine ligands. The pyridyl−amine iridium(III) and rhodium(III) complexes, the corresponding oxidation pyridyl−imine products, and 16-electron pyridyl−amido complexes can be obtained through the change in reaction conditions (nitrogen/adventitious oxygen atmosphere, reaction time, and solvents) and structural variations in the metal and ligand. Overall, the reaction of pyridine−amine ligands with $[(\eta^5\text{-}C_5(CH_3)_5)MCl_2]_2$ (M = Ir or Rh) in the presence of adventitious oxygen afforded the oxidized pyridyl−imine complexes. The possible mechanism for the oxidation of iridium(III) and rhodium(III) amine complexes was confirmed by the detection of the byproduct hydrogen peroxide. Moreover, the formation of pyridyl−amine complexes was favored when nonpolar solvent CH_2Cl_2 was used instead of CH_3OH. The rarely reported complex with $[(\eta^5\text{-}Cp^*)IrCl_3]$ anions can also be obtained without the addition of NH_4PF_6. The introduction of the sterically bulky *i*-Bu group on the bridge carbon of the ligand led to the formation of stable 16-electron pyridyl−amido complexes. The pyridyl−amine iridium(III) and rhodium(III) complexes were also synthesized under a N_2 atmosphere, and no H_2O_2 was detected in the whole process. In particular, the aqueous solution stability and in vitro cytotoxicity toward A549 and HeLa human cancer cells of these complexes were also evaluated. No obvious selectivity was observed for cancer cells versus normal cells with these complexes. Notably, the represented complex **5a** can promote an increase in the reactive oxygen species level and induce cell death via apoptosis.

1. INTRODUCTION

Platinum metal-based anticancer drugs have achieved great success in the treatment of various tumors.[1−3] However, side effects and drug resistance have stimulated exploration of alternative metal complexes.[4−7] Among these complexes, half-sandwich organometallic platinum group metal-based (ruthenium, iridium, rhodium, and osmium) complexes with the piano-stool configuration have been well studied as anticancer agents.[8−28] These complexes have shown promising anticancer activity and some different mechanisms of action (MoAs) with platinum drugs. For example, Sadler and co-workers reported that the high-potency phenylpyridine iridium(III) complexes (Scheme 1, **I**) induced a significant increase in reactive oxygen species (ROS) in cancer cells, which involved catalytic hydride transfer from the coenzyme NADH to oxygen to generate the ROS hydrogen peroxide (H_2O_2).[29,30] Our group has also found that the cationic half-sandwich pyridyl−imine iridium(III) and ruthenium(II) complexes could produce significant levels of ROS, disrupt the mitochondrial membrane, and show potent anticancer activity toward A549 cancer cells (Scheme 1, **II** and **III**).[31,32] Interestingly, some ruthenium(II) complexes achieved good selectivity toward cancer cells and normal cells.[32,33] More recently, we further demonstrated that the metal variation in the zwitterionic pyridyl−imine half-sandwich complexes and the

Received: March 25, 2022
Published: June 23, 2022

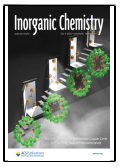

Scheme 1. Half-Sandwich Platinum-Group Metal Complexes Containing a Pyridyl Moiety

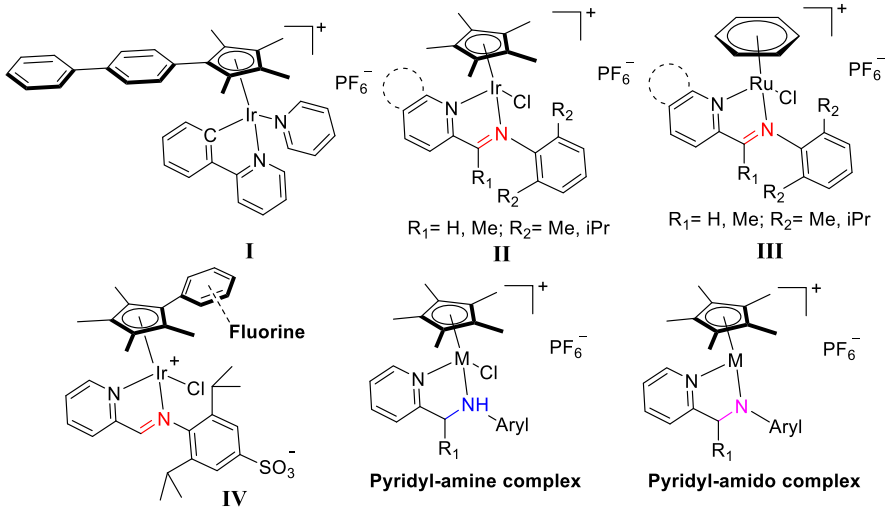

Scheme 2. Synthesis of Ligands 1a−1d

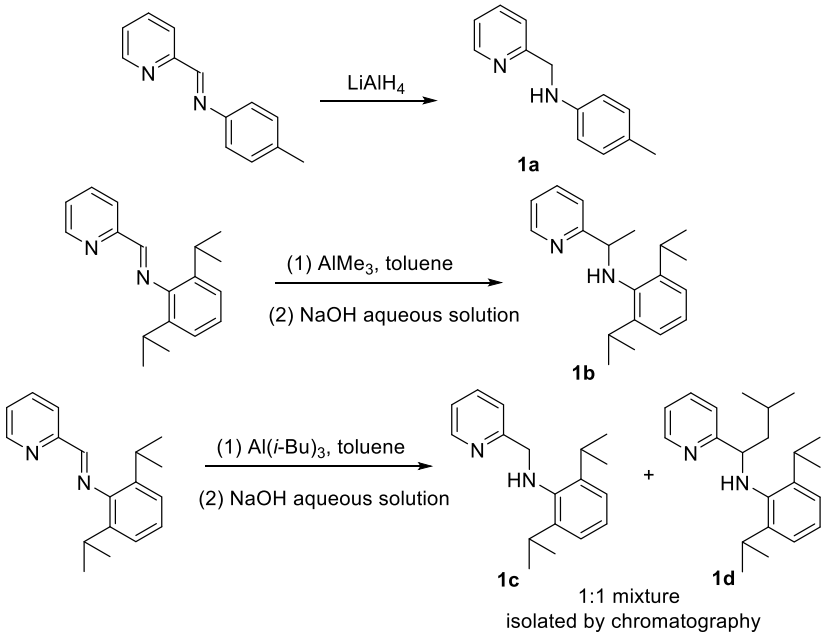

introduction of fluorinated substituents resulted in a significant increase in the anticancer activity (Scheme 1, **IV**).[34−36] Notably, the coordination fashion of the abovementioned pyridyl−imine half-sandwich iridium(III) complexes was imine-metal. Along this line, we became interested in expanding our investigation to the synthesis and biological evaluation of the corresponding amine−metal and amido−metal complexes (Scheme 1).

In this present study, we initially intended to synthesize pyridyl−amine iridium(III) and rhodium(III) complexes (Scheme 1, pyridyl−amine complex) by the reaction of pyridyl−amine ligands with the corresponding iridium(III) and rhodium(III) dimer precursors. However, the unexpected products of the oxidized imine complexes were generated under the conditions of adventitious molecular oxygen, especially the reaction of dimer precursor $[(\eta^5\text{-Cp}^*)\text{IrCl}_2]_2$ ($\text{Cp}^* = \text{C}_5(\text{CH}_3)_5$) with pyridyl−amine ligands in the absence of NH_4PF_6 afforded rarely reported complex with $[(\eta^5\text{-Cp}^*)\text{IrCl}_3]$ anions.[37,38] Moreover, the pyridyl−amine iridium(III) and rhodium(III) complexes and the corresponding oxidation pyridyl−imine products can be obtained respectively in good yields by adjusting reaction conditions (nitrogen/adventitious oxygen atmosphere, reaction time, and solvents). Notably, when a sterically demanding iso-butyl group on the bridge carbon between the pyridyl moiety and amine moiety was introduced, no oxidation was observed and a stable 16-electron pyridyl−amido complex was generated (Scheme 1, pyridyl−amido complex).

2. RESULTS AND DISCUSSION

2.1. Synthesis of Ligands. Pyridine−amine ligands **1a−1d** were synthesized in good yields by a reduction reaction of pyridine−imine ligands with $LiAlH_4$, $AlMe_3$,[39] and $Al(i\text{-Bu})_3$ (Scheme 2). The steric hindrance of the substituents on the bridge carbon between the pyridyl moiety and the amine moiety can be tuned using these different reduction agents. Interestingly, when $Al(i\text{-Bu})_3$ was employed to synthesize **1d**, a mixture of **1c** and **1d** (ca. 1:1 molar ratio) was obtained, and they could

https://doi.org/10.1021/acs.inorgchem.2c00984
Inorg. Chem. 2022, 61, 10051−10065

Scheme 3. Synthesis of (i) Pyridyl−Imine or (ii) Pyridyl−Amine Complexes in the Presence of Small Amounts of Adventitious Molecular Oxygen When the Polar Solvent CH_3OH Was Used

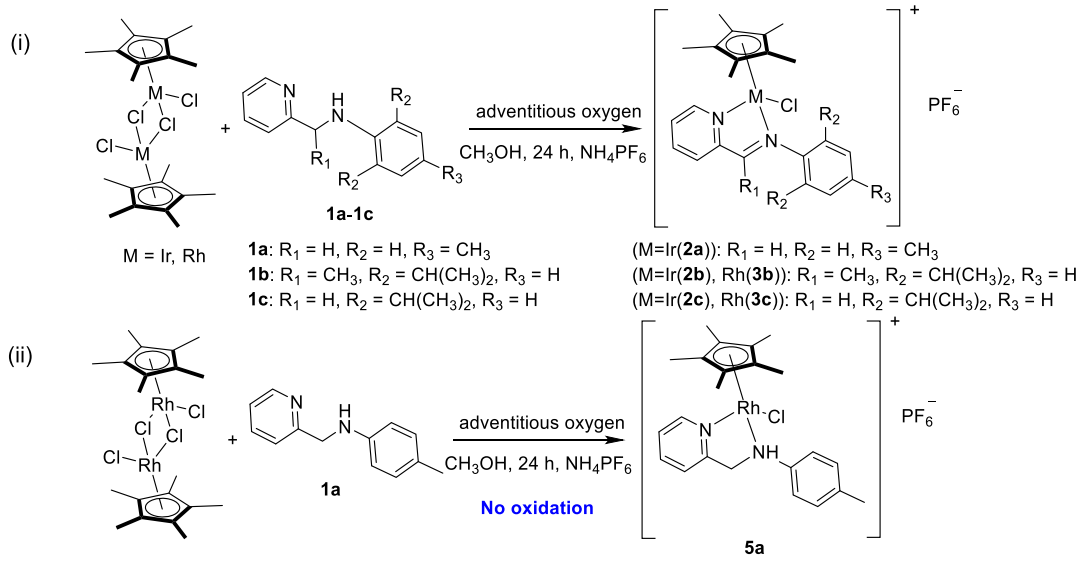

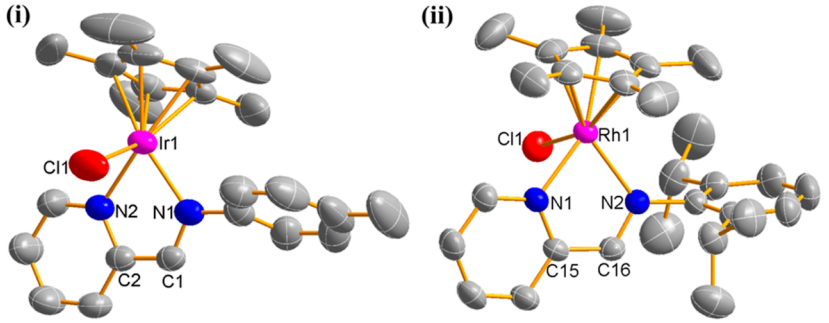

Figure 1. X-ray crystal structure of complexes (i) **2a** and (ii) **3c** with the thermal ellipsoids drawn at the 50% probability level. The hydrogen atoms and PF_6^- anions have been omitted for clarity. (i) Bond angles around Ir(III) ions (deg): N1−Ir1−N2 = 76.07(14). Bond lengths (Å): Ir1−C(centroid) = 1.8001, Ir1−N1 = 2.108(3), Ir1−N2 = 2.101(3), Ir1−Cl1 = 2.3713(11), and C1−N1 = 1.275(5); (ii) bond angles around Rh (III) ions (deg): N1−Rh1−N2 = 76.59(11). Bond lengths (Å): Rh1−C(centroid) = 1.8045, Rh1−N1 = 2.114(3), Rh1−N2 = 2.142(3), Rh1−Cl1 = 2.4081(9), and C16−N2 = 1.286(4).

be readily separated by chromatography. The possible mechanism for the production of **1c** and **1d** mixture is shown in Scheme S1. The intermediate pyridyl−amido aluminum(III) complex was generated by the reaction of Al(*i*-Bu)$_3$ with the pyridyl−imine compound. The mixture was then quenched with NaOH aqueous solution, and **1d** was finally obtained. In the meantime, β-H elimination of Al(*i*-Bu)$_3$ at reflux temperature may result in the formation of $[Al(i\text{-}Bu)_2(\mu\text{-}H)]_2$.[40] Subsequently, the in situ treatment of $[Al(i\text{-}Bu)_2(\mu\text{-}H)]_2$ with the pyridine−imine compound led to the generation of **1c**. This mechanism was further supported by the observation that only **1b** was produced when $AlMe_3$ (without β-H) was employed.

2.2. Oxidative Dehydrogenation of Amine to Imine Complexes. The initial design was to synthesize cationic half-sandwich pyridyl−amine iridium(III) and rhodium(III) complexes. The reactions of pyridine−amine ligands with $[(\eta^5\text{-}Cp^*)MCl_2]_2$ (M = Ir or Rh, Cp* = $C_5(CH_3)_5$) were performed for 24 h and in the presence of small amounts of adventitious oxygen (the solution was not degassed with nitrogen), which was usually employed to synthesize half-sandwich iridium(III) and rhodium(III) analogues in our previous work.[31,35,36] However, the corresponding oxidation products, that is, pyridyl−imine iridium(III) and rhodium(III) complexes (**2a**−**2c** and **3b**−**3c**, Scheme 3(i)), were cleanly obtained in 64−78% isolated yields. Notably, the pyridyl−amine complex **5a** was synthesized under the same conditions without the formation of the oxidized pyridyl−imine complex (Scheme 3(ii) vs Scheme 3(i)), which indicated that the oxidation reaction in this system could be attributed to the combinatorial action of the metal center and the structure of the pyridyl−amine ligand. Purity and identity of **2a**−**2c** and **3b**−**3c** were confirmed by ^{1}H and ^{13}C NMR (Figures S8−S17), mass spectrometry (Figures S40−S44), elemental analysis (Figures S54−S57), and single-crystal X-ray crystallography. In order to confirm the formation of the oxidized pyridyl−imine complexes, the pyridyl−imine iridium(III) and rhodium(III) complexes were also prepared by the reactions of the corresponding pyridine−imine ligands with $[(\eta^5\text{-}Cp^*)MCl_2]_2$ (M = Ir or Rh), and they showed the same NMR spectra with the abovementioned complexes generated using pyridine−amine ligands (Figures S34−S37).

The crystalline samples of **2a** and **3c** suitable for X-ray diffraction analysis were obtained by slow diffusion of hexane (or the mixture of hexane and diethyl ether) in a dichloromethane (or acetonitrile) solution. The selected bond lengths are given in Figure 1. Planar five-member metallacycles were observed in both **2a** (Ir1−N1−C1−C2−N2) and **3c** (Rh1−N1−C15−

https://doi.org/10.1021/acs.inorgchem.2c00984
Inorg. Chem. 2022, 61, 10051−10065

Scheme 4. Synthesis of Pyridyl−Imine or Pyridyl−Amine Complexes in the Presence of Small Amounts of Adventitious Molecular Oxygen (i) under the Reaction Time of 2 h or (ii and iii) in the Non-Polar Solvent CH_2Cl_2

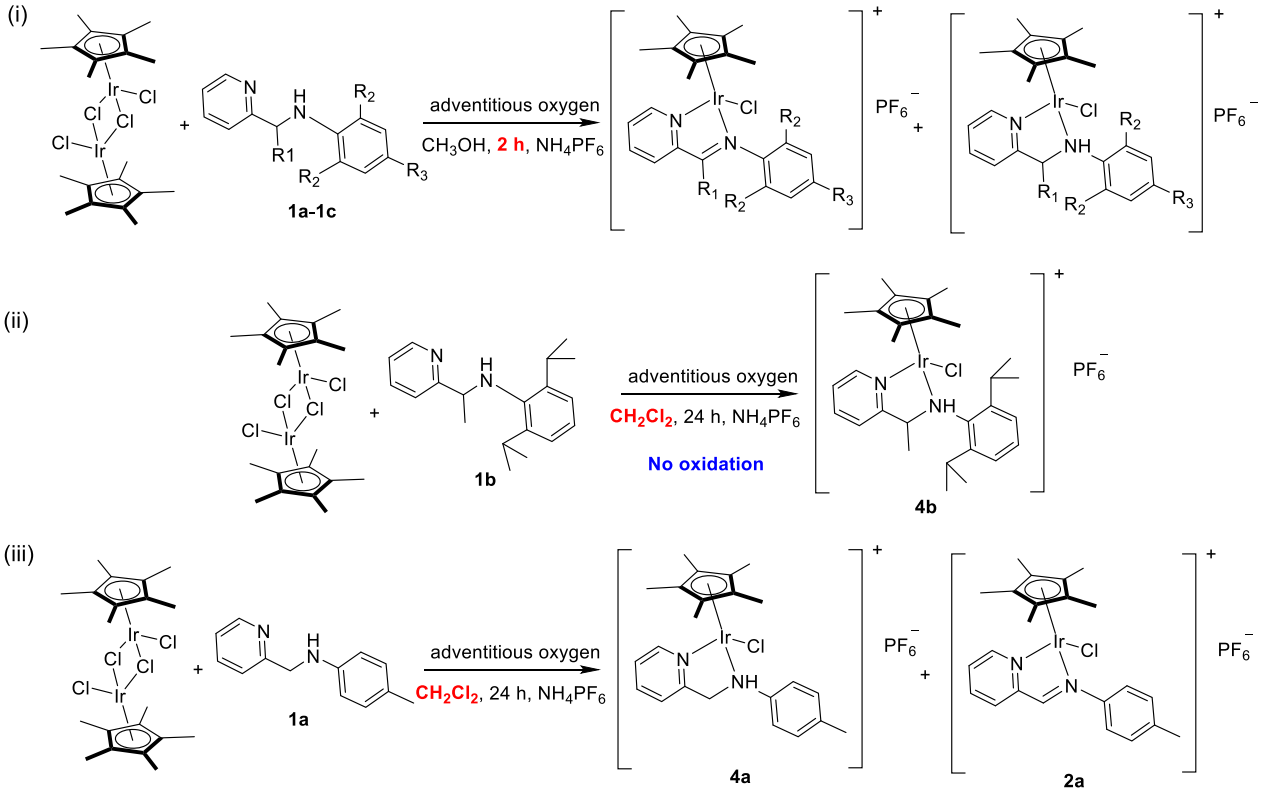

Scheme 5. Synthesis of Complex 6 with $[(\eta^5\text{-Cp*})IrCl_3]$ Anion

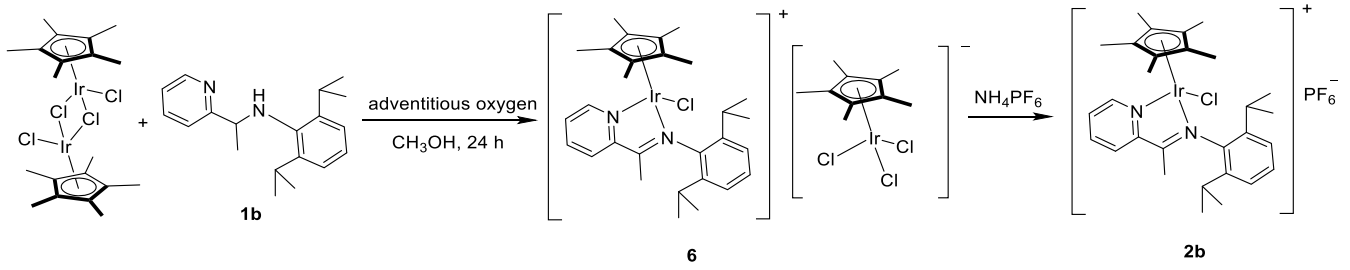

C16−N2) due to the coplanar structure between the pyridyl moiety and C═N bond. Moreover, the C1−N1 (1.275(5) Å) (**2a**) and C16−N2 (1.286(4) Å) (**3c**) distances were in agreement with double bonds of C═N. The bond angles and lengths are similar to those reported for pyridyl−imine iridium(III) and rhodium(III) complexes obtained by the reaction of pyridine−imine ligands with $[(\eta^5\text{-Cp*})MCl_2]_2$.[31,41] Previous studies have shown that some pyridyl−amine ruthenium(II) and iridium(III) complexes can be oxidized to the pyridyl−imine complexes when molecular oxygen is not totally eliminated.[42,43] The acidic N−H proton on the pyridyl−amine ligands can promote the production of the oxidized imine complexes.[42,44,45] According to the reported mechanism by Gómez et al. for the oxidation of amine to imine ruthenium(II) complexes,[42] the proposed steps in this system are shown in Scheme S2. In the process of preparing **2a**−**2c**, **3b**, and **3c**, the formation of H_2O_2 in the oxidation reaction was unequivocally confirmed in a peroxide test using a Quantofix test stick (Scheme S2), which supported this oxidation mechanism.

Furthermore, when the reaction time changed from 24 to 2 h, a mixture of pyridyl−imine and pyridyl−amine complexes was obtained (Scheme 4(i) vs Scheme 3(i)), which further proved the oxidation mechanism. In this case, we were unable to separate two kinds of complexes by standard purification methods. The oxidation reaction was also dependent on the solvent used in this reaction. For example, when the non-polar solvent CH_2Cl_2 was used instead of CH_3OH, the formation of the imine complex **2b** was not observed and the amine complex **4b** was cleanly obtained (Scheme 4(ii) vs Scheme 3(i)). In another case, when **1a** was employed to react with $[(\eta^5\text{-Cp*})IrCl_2]_2$ in CH_2Cl_2, a mixture of the amine complex **4a** (more than 50% determined by ^1H NMR analysis) and the imine complex **2a** was generated (Scheme 4(iii) vs Scheme 3(i)). It seemed reasonable that the non-polar CH_2Cl_2 made the deprotonation of the amine complexes difficult, that is, lowered the acidity of the N−H proton and thus prevented or suppressed the formation of the oxidized imine complexes.

The reactions of pyridyl−amine ligands with $[(\eta^5\text{-}C_5(CH_3)_5)MCl_2]_2$ without the addition of NH_4PF_6 were also performed under the same reaction conditions. The oxidation product was also completely obtained. This pyridyl−imine iridium(III) complex showed a rarely reported structure with

https://doi.org/10.1021/acs.inorgchem.2c00984
Inorg. Chem. 2022, 61, 10051−10065

$[(\eta^5\text{-Cp*})IrCl_3]$ anions (Scheme 5, **6**) and could be generated cleanly even when the iridium(III) dimer $[(\eta^5\text{-Cp*})IrCl_2]_2$ was reacted with 2 equiv of the pyridyl−amine ligand. Kennedy and Smith have shown that the more weakly coordinating ligand could lead to the incomplete dissociation of the precursor $[(\eta^5\text{-Cp*})IrCl_2]_2$ and afford anionic and cationic ion pairs in their system.[37] However, in most cases, half-sandwich iridium complexes with Cl^- as counteranions were obtained in the absence of an exogeneous source of a weakly coordinating anion (e.g., PF_6^-).[27,28,46] For example, when the common N,*N*-chelating ligands 1,10-phenanthroline (phen), 2,2′-bipyridine (bpy) and ethylenediamine (en) were employed to react with $[(\eta^5\text{-}C_5(CH_3)_5)IrCl_2]_2$ without addition of NH_4PF_6, the formation of half-sandwich iridium complexes with Cl^- as non-coordinating counteranions was observed.[27] Thus, the generation of rare $[(\eta^5\text{-Cp*})IrCl_3]$ anions seemed to be associated with the relative binding strengths of the chelating N-donor ligands. This complex with $[(\eta^5\text{-Cp*})IrCl_3]$ anions was very stable in DMSO-d_6 and $CDCl_3$ solution over extended periods. The ^{1}H NMR spectra of complex **6** showed two characteristic peaks (1.50 and 1.61 ppm) corresponding to the proton of the Cp* in the cationic part and anionic part, respectively (Figure S30). Moreover, the presence of two molar equivalents of bound Cp* per mol ligand was also observed.

Complex **6** was also confirmed by elemental analysis and single-crystal X-ray crystallography (Figure 2). Similar to complexes **2a** and **3c**, the cationic part of complex **6** adopted the typical piano-stool conformation with the five-membered metallocycle formed by the coordination of the pyridyl−imine ligand. The Ir−N distances were also comparable to those previously reported for monometallic iridium(III) pyridyl−imine complexes containing counteranion PF_6^-.[31] The anion

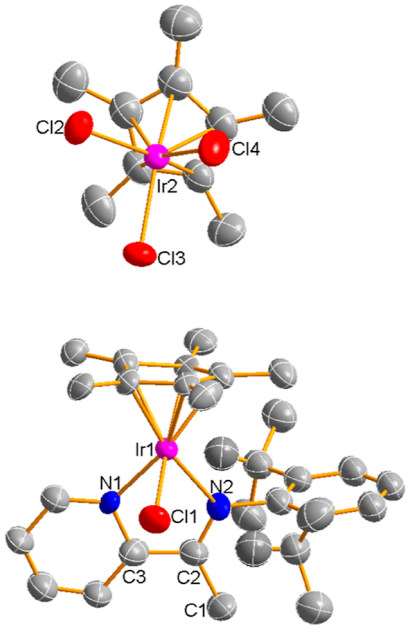

Figure 2. X-ray crystal structure of complex **6** with the thermal ellipsoids drawn at the 50% probability level. The hydrogen atoms have been omitted for clarity. Bond angles around Ir(III) ion (deg): N1−Ir1−N2 = 75.8(7), Cl2−Ir2−Cl3 = 90.2(2), Cl2−Ir2−Cl4 = 86.7(2), and Cl3−Ir2−Cl4 = 88.1(2). Bond lengths (Å): Ir1−C(centroid) = 1.8127, Ir1−N1 = 2.089(18), Ir1−N2 = 2.102(16), Ir1−Cl1 = 2.393(5), and C2−N2 = 1.312(18); Ir2−C(centroid) = 1.7623, Ir2−Cl2 = 2.391(6), Ir2−Cl3 = 2.422(6), and Ir2−Cl4 = 2.424(7).

$[(\eta^5\text{-Cp*})IrCl_3]$ displayed the same piano-stool geometry with the η^5-Cp* ligand occupying three coordination sites and the three chloride atoms occupying three facial positions. The average of Ir−Cl bond lengths was 2.4123 Å. The distance (1.7623 Å) between the centroid of the Cp* ring and the metal center was slightly shorter than in the cationic parts (1.8127 Å). The reaction of complex **6** with NH_4PF_6 afforded the monometallic complex **2b** with PF_6^- as counteranions, indicating that NH_4PF_6 was simply a reaction reagent for anion exchange in the oxidation process.

2.3. Synthesis and Reactivity of Amido Complexes. The most notable observation was the formation of pyridyl−amido complex **7** when the sterically bulky *i*-Bu group on the bridge carbon of the ligand was employed instead of H and CH_3 substituents (Scheme 6). The reaction conditions were the same as those for complexes **2a**−**2c**. However, the formation of the oxidized imine complex was not observed, and the amido complex **7** was cleanly obtained in 70% isolated yield. This type of half-sandwich 16-electron complex was rarely reported. Notably, the β hydrogen (C*H*(*i*-Bu), H proton at the β position to the metal) on the bridge carbon existed in our system. The previously reported stable 16-electron ruthenium(II) analogues could be obtained only when the β hydrogen atom was avoided and the deprotonating agents (e.g., NaOMe) were added.[42] Thus, the successful synthesis of stable pyridyl−amido iridium(III) complexes containing β hydrogen atoms in this system was likely due to the high steric requirements (*i*-Bu group) on the bridge carbon. The identity and purity of complex **7** were determined by ^{1}H and ^{13}C NMR (Figures S32 and S33), mass spectrometry (Figure S53), elemental analysis, and single-crystal X-ray crystallography. The molecular structure of complex **7** is shown in Figure 3. Complex **7** adopted five-coordinated (16-electron) piano-stool geometry, and no leaving group Cl^- bound to the metal center. Furthermore, a nonplanar five-member metallacycle was observed in complex **7**, and the C6−N2 (1.470 Å) distance was in agreement with the single bond of C−N.

The ^{1}H NMR spectra of pyridyl−amido complex **7** exhibited no obvious change over 24 h, suggesting that this type of iridium(III) complex was fairly stable in $CDCl_3$ or DMSO-d_6. Previous studies have displayed that the reactions of 16-electron half-sandwich iridium(III) and ruthenium(II) complexes with a series of two-electron donors can produce stable 18-valence electron compounds.[47,48] When PPh_3, CH_3CN, or a CO atmosphere was introduced in a NMR tube containing a $CDCl_3$ solution of **7**, no additional ^{1}H NMR peaks were observed over a period of 20 h, indicating that PPh_3, CH_3CN, and CO did not react with **7** (Figures S58−S60). The stable nature of **7** may also support the oxidation mechanism shown in Scheme S2. The amido complex with the bulky *i*-Bu group might have been formed in situ by deprotonation of the amine complex in step (i) and showed a very stable nature. As a result, the step (ii) (the oxidation of the amido complex by oxygen) could be stopped. On the other hand, the ^{1}H NMR chemical shifts as a measure of the N−H acidity of the respective N−H proton for **1a**−**1d** could be considered.[49] The chemical shift of the N−H proton in **1d** with the bulky *i*-Bu group (ca. 3.99 ppm) was lower than that of the N−H protons in **1a**−**1c** (4.05−4.61 ppm) (Figures S2-S6). This means a lower acidity of the N−H proton in **1d**, which could also be considered as a plausible mechanism for the absence of the oxidation. The reaction of **1d** with $[(\eta^5\text{-Cp*})RhCl_2]_2$ was also performed under the same conditions. This reaction gave one new point on the thin-layer chromatography plates, and complete purification seemed to

https://doi.org/10.1021/acs.inorgchem.2c00984
Inorg. Chem. 2022, 61, 10051−10065

Scheme 6. Synthesis of 16-Electron Pyridyl−Amido Complex 7 in the Presence of Small Amounts of Adventitious Molecular Oxygen

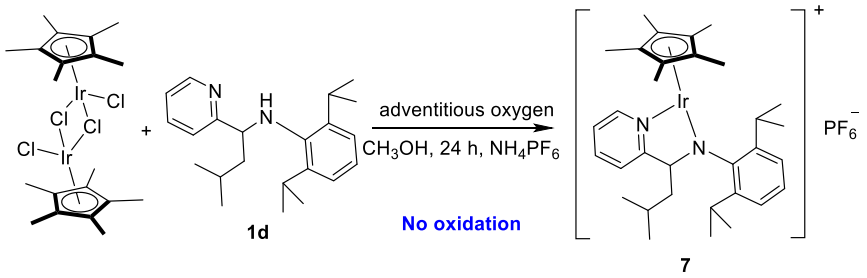

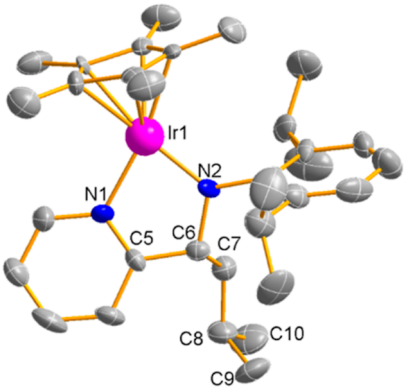

Figure 3. X-ray crystal structure of complex **7** with the thermal ellipsoids being drawn at the 50% probability level. The hydrogen atoms and PF_6^- anions have been omitted for clarity. Bond angles around Ir(III) ions (deg): N1−Ir1−N2 = 78.6(5). Bond lengths (Å): Ir1−C (centroid) = 1.7966, Ir1−N1 = 2.053(12), Ir1−N2 = 1.907(13), and C6−N2 = 1.470(17).

be achieved. The ESI-MS analysis showed the presence of the corresponding 16-electron complexes. However, ^{1}H NMR spectra of the products were too complicated for the assignment of signals, indicating that this complex may be unstable and other species were formed in solution.

2.4. Synthesis and Characterization of Amine Complexes. The pyridyl−amine complexes **4a−4c** and **5a−5c** were synthesized (Scheme 7) in 60−71% isolated yields by the reaction of the precursors $[(\eta^5\text{-Cp}^*)\text{IrCl}_2]_2$ or $[(\eta^5\text{-Cp}^*)\text{RhCl}_2]_2$ with pyridyl−amine ligands **1a−1c** in methanol or CH_2Cl_2 under a nitrogen atmosphere (the solution was degassed with nitrogen in the whole process). In this case, no H_2O_2 was detected in the peroxide test using a Quantofix test stick (Figure S61). Except for **5a**, these pyridyl−amine complexes were not stable in $CDCl_3$ or DMSO-d_6 solution with adventitious oxygen, and the oxidized pyridyl−imine complex could be observed over time. This observation is also consistent with the abovementioned proposed oxidation mechanism. Characterization of these complexes was performed by ^{1}H and ^{13}C NMR (Figures S18−S29), mass spectrometry (Figures S45−S50), elemental analysis, (Figures S54−S57) and single-crystal X-ray crystallography (Figure 4). Notably, the secondary amine ligands have chiral nitrogen atoms, and the nonplanar five-membered chelate ring of the ligand is also a chiral entity.[42,50] Hence, most of these complexes were found to be a mixture of diastereomers in solution, which can be confirmed from the distinct peaks for the major and minor isomers. It should be noted that the diastereomeric behavior of the similar amine ruthenium(II) and iridium(III) complexes has been reported in detail.[42,43] The two characteristic peaks in the ^{1}H NMR spectra for these amine complexes were at ca. 3.64−5.64 ppm and ca. 6.51−7.34 ppm, corresponding to the protons of the CH-R group (H on the bridge carbon, R = H or CH_3) and N−H protons, respectively. In the case of **4a**, **5a**, **4c**, and **5c**, the signals of each proton of the CH_2 group displayed separately due to the presence of the two diastereomeric protons, which was also in agreement with the previously reported amine complexes.[43] In contrast to the abovementioned imine complexes **2a** and **3c**, which showed planar five-member metallacycles, nonplanar five-member metallacycles were observed in these amine complexes **4a** (Ir1−N1−C11−C12−N2), **5a** (Rh1−N1−C2−C1−N2), and **5b** (Rh1−N1−C3−C2−N2) due to the coordination of sp^3 nitrogen (Figure 4). The C11−N1 (1.466(5) Å) (**4a**), C1−N2 (1.466(7) Å) (**5a**), and C2−N2 (1.504(5) Å) (**5b**) distances were longer than those in imine complexes (C═N bonds in **2a** and **3c**: 1.275−1.286 Å) and in agreement with single bonds of C−N. Moreover, the coordination of leaving group Cl^- to the metal center was observed. These results were consistent with the amine−metal coordination mode.

Scheme 7. Synthesis of Pyridyl−Amine Complexes Under a Nitrogen Atmosphere

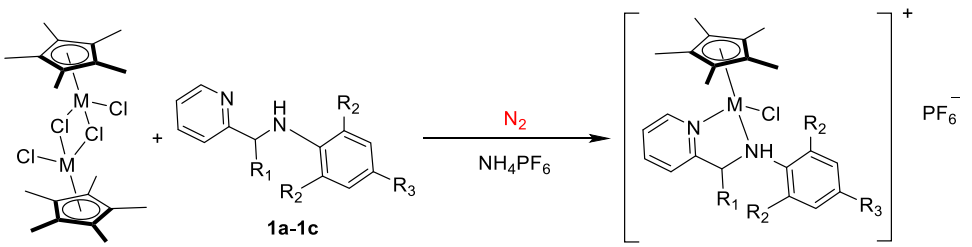

M = Ir, Rh

(M=Ir(**4a**), Rh(**5a**)): R_1 = H, R_2 = H, R_3 = CH_3
(M=Ir(**4b**), Rh(**5b**)): R_1 = CH_3, R_2 = $CH(CH_3)_2$, R_3 = H
(M=Ir(**4c**), Rh(**5c**)): R_1 = H, R_2 = $CH(CH_3)_2$, R_3 = H

https://doi.org/10.1021/acs.inorgchem.2c00984
Inorg. Chem. 2022, 61, 10051−10065

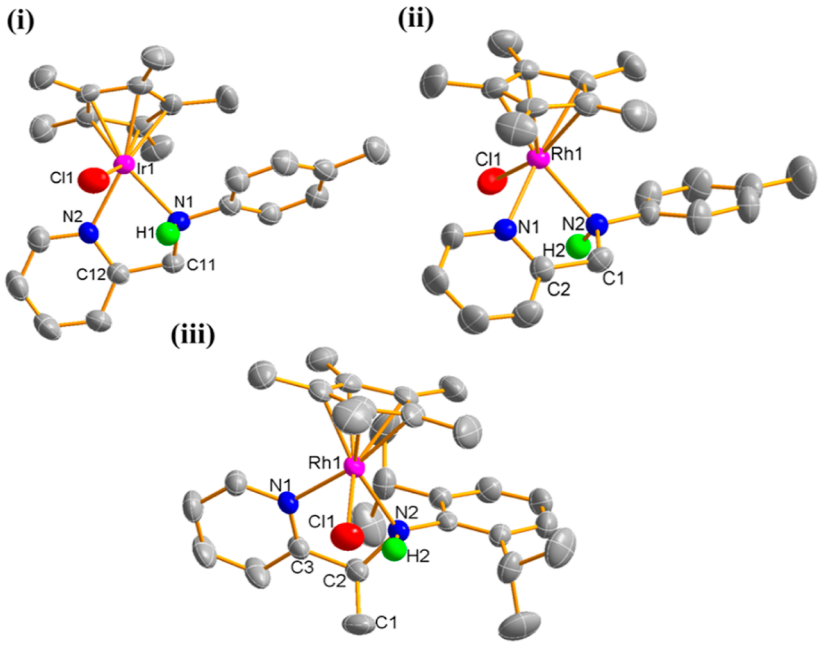

Figure 4. X-ray crystal structures of complexes (i) **4a**, (ii) **5a**, and (iii) **5b** with the thermal ellipsoids drawn at the 50% probability level. Some hydrogen atoms and the PF_6^- anion have been omitted for clarity. (i) Bond angles around Ir(III) ions (deg): N1−Ir1−N2 = 75.21(12). Bond lengths (Å): Ir1−C(centroid) = 1.7899, Ir1−N1 = 2.174(3), Ir1−N2 = 2.105(3), and Ir1−Cl1 = 2.3873(11), C11−N1 = 1.466(5); (ii) Bond angles around Rh(III) ions (deg): N1−Rh1−N2 = 74.88(18). Bond lengths (Å): Rh1−C(centroid) = 1.7661, Rh1−N1 = 2.096(5), Rh1−N2 = 2.179(5), Rh1−Cl1 = 2.3738(17), and C1−N2 = 1.466(7); (iii) bond angles around Rh(III) ions (deg): N1−Rh1−N2 = 77.33(13). Bond lengths (Å): Rh1−C(centroid) = 1.7886, Rh1−N1 = 2.105(3), Rh1−N2 = 2.238(3), Rh1−Cl1 = 2.3763(13), and C2−N2 = 1.504(5).

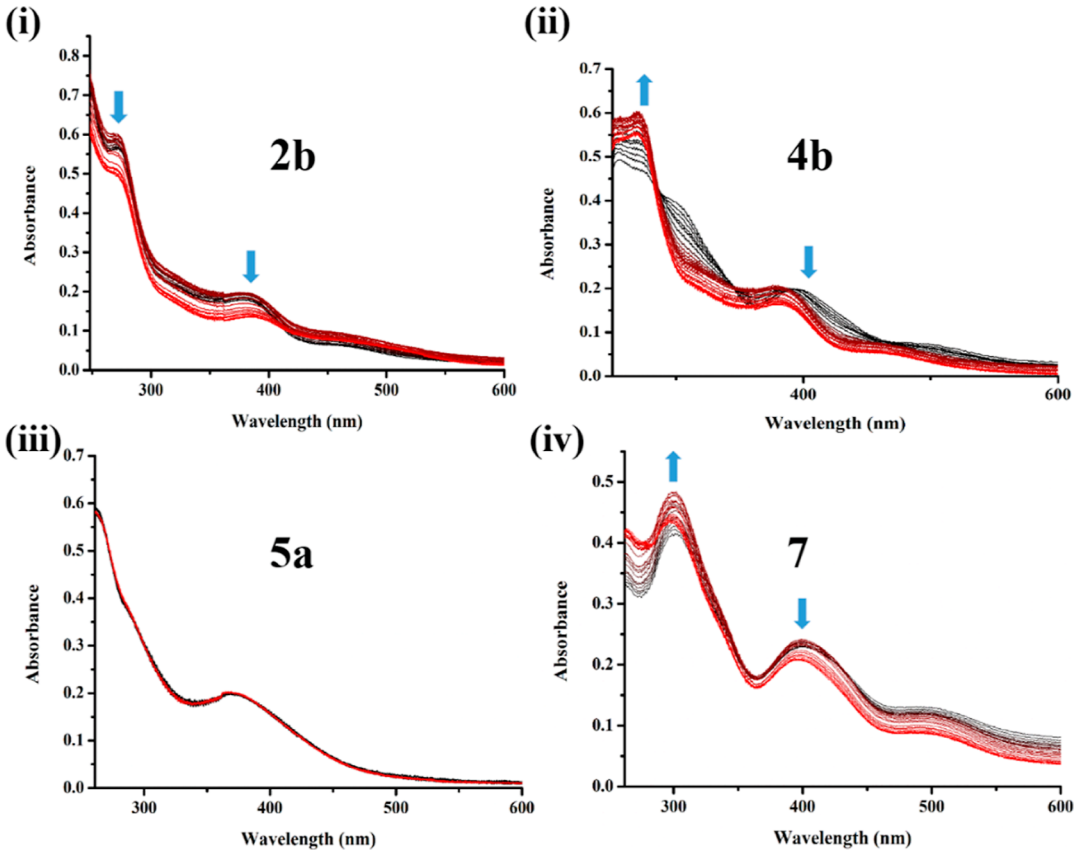

Figure 5. UV−vis spectra for complexes **2b**, **4b**, **5a**, and **7** recorded over a period of 24 h at 37 °C: (i) solution in 30% DMSO/70% PBS (v/v) of **2b**, (ii) solution in 30% DMSO/70% PBS (v/v) of **4b**, (iii) solution in 30% DMSO/70% PBS (v/v) of **5a**, and (iv) solution in 30% DMSO/70% PBS (v/v) of **7**.

https://doi.org/10.1021/acs.inorgchem.2c00984
Inorg. Chem. 2022, 61, 10051−10065

2.5. Aqueous Stability. It is essential to evaluate the stability of the metal complexes in aqueous media and under physiological conditions for drug development. Thus, the stability of the complexes in this system was assessed using UV−visible spectrophotometry in 70% phosphate buffered saline (PBS) (PBS is prepared from water pH: ca. 7.2)/30% DMSO (v/v) at 37 °C (Figures 5 and S62). Notably, we have previously reported that the similar pyridyl−imine iridium(III) complexes, which were prepared by the reactions of the corresponding pyridine−imine ligands with $[(\eta^5\text{-Cp}^*)MCl_2]_2$ rather than the pyridine−amine ligand-involved oxidation reaction, could undergo hydrolysis of M−Cl, that is, Cl^-/H_2O exchange in aqueous media,[31] which represented an activation step for some metal-based anticancer complexes since aqua complex M−OH_2 is usually more active than the chloride complex M−Cl.[27,51] The absorption intensities changed in the spectra of the pyridyl−imine complexes (**2a−2c**, **6**, and **3b−3c**) in this system, and no obvious shift in the absorption bands was tested over a period of 24 h (e.g., **2b** in Figure 5(i)). This result was in agreement with our previous observation of the pyridyl−imine iridium(III) analogues[31] and indicated that the pyridyl−imine iridium(III) complexes **2a−2c** and **6** and rhodium(III) complexes **3b−3c** in this system also underwent hydrolysis under the test conditions. Conversely, a significant change in the absorption bands (both in the pattern and the intensity) was observed for the pyridyl−amine complexes over a period of 24 h (e.g., **4b** in Figure 5(ii)), which may be associated with the formation of the oxidized pyridyl−imine complex. However, the oxidation process and hydrolysis of M−Cl bonds may occur simultaneously in this case, and we could not identify any bands corresponding to any of the chloride or aqua complexes. This speculation was further supported by the observation that no obvious shift in the absorption bands was found in the spectra of **5a** due to its resistance to oxidation reaction (Figure 5(iii)), which was consistent with the result that **5a** was synthesized without the formation of the oxidized imine complex after 24 h. Moreover, only minor changes in intensity were observed in the UV−vis spectra of **5a**, also evidencing the stability of **5a** in aqueous solutions. To confirm the stability of **5a**, ^{1}H NMR analysis was also performed in 85% DMSO-d_6/15% PBS (PBS was prepared from D_2O) solutions at 37 °C (Figure S63). There was no change in the spectra of **5a**, and the assignment of protons was completely consistent with its molecular structure, which further evidenced the stability of **5a** in aqueous media. As mentioned above, amido complex **7** was stable in DMSO-d_6 solution and showed no reactivity toward two-electron donors (PPh_3, CH_3CN, and CO). However, some changes in absorption intensity in the UV−vis spectra of **7** were observed after 24 h (Figure 5(iv)), demonstrating that H_2O was likely to bind to the 16-electron parent complex **7** and the partial 18-electron aquated complex (Ir−OH_2) may have formed in aqueous solutions. Additionally, the ^{1}H NMR spectra of **7** in 85% DMSO-d_6/15% PBS solutions at 37 °C showed some changes over time, which further proved this speculation (Figure S64). However, it can be estimated that most of the parent complex was present in 85% DMSO-d_6/15% PBS solution over 24 h. The stability of these represented complexes **2b**, **4b**, **5a**, and **7** in the cell culture media [Dulbecco's modified Eagle medium with 30% dimethyl sulfoxide (DMSO) to attain full dissolution] was also determined. The stability behavior was similar with the abovementioned results obtained in PBS buffer mixture except **7** (Figure S1), which exhibited obvious changes over time, suggesting that this 16-electron complex was likely susceptible to bind to the constituents of the cell culture medium.

2.6. In Vitro Cytotoxicity. Previously, we have synthesized the pyridyl−imine iridium(III) and ruthenium(II) complexes through the reactions of the pyridyl−imine ligands with the corresponding metal precursors, and these complexes displayed appreciable biological activities.[31,32] Hence, we sought to expand the investigation to the pyridyl−imine rhodium(III) complexes prepared in this work. Moreover, to the best of our knowledge, the biological activity of pyridyl−amido and pyridyl−amine iridium(III) and rhodium(III) complexes has never been investigated to date. As mentioned above, most of the pyridyl−amine complexes would suffer from the oxidation reaction if oxygen (even adventitious oxygen) is not rigorously excluded. Thus, **5a** would be more suitable as a typical complex for this exploratory work due to its resistance to oxidation reaction. On the basis of these considerations, the cytotoxicity of these complexes in the A549 lung cancer cell line and HeLa cervical cancer cell line was investigated using 3-[4,5-dimethylthiazol-2-yl]-2,5 diphenyl tetrazolium bromide (MTT) assay using cisplatin as the positive control (Table 1).

Table 1. In Vitro Cytotoxic Activity of the Complexes after 48 h of Incubation in Cancer and Normal Cell Lines and Comparison with Cisplatin[a]

	IC_{50} (μM)			
complex	A549	HeLa	BEAS-2B	selectivity index[b]
2a	23.2 ± 0.5	35.1 ± 1.2	45.5 ± 0.6	1.96
2b	29.8 ± 0.3	17.5 ± 0.2	35.3 ± 0.3	1.18
2c	25.1 ± 0.4	21.7 ± 0.3	26.7 ± 0.5	1.06
3b	37.1 ± 0.3	29.3 ± 0.7	37.8 ± 0.1	1.02
3c	30.3 ± 0.1	38.6 ± 0.3	47.1 ± 0.4	1.55
5a	40.1 ± 0.9	16.3 ± 0.3	26.2 ± 1.1	0.65
6	22.5 ± 0.5	13.6 ± 0.1	32.2 ± 0.3	1.43
7	>100	>100	-	-
cisplatin	21.3 ± 1.7	7.5 ± 0.2	42.0 ± 2.3	1.97

[a]The cytotoxicity is expressed as the IC_{50} values (μM) ± standard deviations (n = 3). [b]Selectivity index represents the IC_{50} ratio of BEAS-2B normal cells to A549 cancer cells. (-) indicates no data are available.

It should be noted that no cytotoxic activity (IC_{50} > 100 μM, IC_{50}: dose at which 50% cellular growth was inhibited) was observed for all of the ligands and metal dimer precursors used in this work (Table S8). Thus, the observed cytotoxicity against the tested cancer cells was attributed to the chelation. The pyridyl−imine iridium(III) complexes **2a−2c** and **6** showed the cytotoxicity toward A549 and HeLa cells with IC_{50} values ranging from 13.6 to 35.1 μM, which were comparable to those of cisplatin and our previously reported pyridyl−imine iridium-(III) analogues.[31] The complex **6** with $[(\eta^5\text{-Cp}^*)IrCl_3]$ anion was more active than the corresponding monometallic complex **2b**, indicating that the counteranion also affected the cytotoxicity of these complexes. Notably, the counteranion effect has also been found by our group for the bioactive half-sandwich iridium(III) complexes bearing the chelating bipyridine ligands.[28] Changing the metal center from iridium(III) to rhodium(III) slightly decreased the cytotoxicity of the pyridyl−imine complexes (e.g., **2b** vs **3b**). The 16-electron amido complex **7** gave the IC_{50} value greater than 100 μM and thus was deemed as inactive. Although the MoA was not clear for this amido iridium(III) complex, we speculated that the specific 16-

https://doi.org/10.1021/acs.inorgchem.2c00984
Inorg. Chem. 2022, 61, 10051−10065

electron coordination mode of 7 and its instability in cell culture medium were responsible for the low cytotoxicity. In addition, the amine complex **5a** displayed almost a similar IC_{50} value toward A549 cancer cells and showed a slightly higher cytotoxicity against HeLa cancer cells in comparison with the imine rhodium(III) complexes (**3b** and **3c**). Overall, it seemed that the changing of the coordination mode from imine−metal to amine−metal was not sensitive to the cytotoxicity of the complexes in this system. MTT assay was also performed with noncancerous BEAS-2B. Unfortunately, no obvious selectivity was observed for cancer cells versus normal cells with these complexes, and the IC_{50} values of these complexes (26.2−47.1 μM) were also comparable to or lower than those of cisplatin (42.0 μM). Thus, the ordinary toxicity of these complexes cannot be excluded.

2.7. ROS Determination. It should be noted that our previously reported pyridyl−imine iridium(III) and ruthenium(II) complexes can increase ROS levels significantly in A549 cells.[31−33,52] Thus, we also became interested in the effect of changing the coordination mode from imine complexes to amine complexes on ROS production. The levels of ROS in A549 cells induced by **5a** at the concentrations of 0.25, 0.5, and 1 × IC_{50} were determined using an ROS assay kit (Figures 6 and

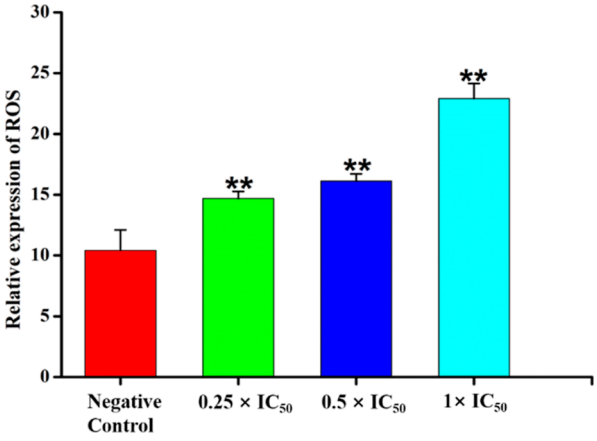

Figure 6. Analysis of ROS levels using a fluorescence microscope after A549 cells were treated with **5a** for 24 h at 37 °C and stained with DCFH-DA. *p*-values were calculated after a *t* test against the negative control data, $^{**}p < 0.01$.

S65). Compared to untreated cells, an increase in concentration-dependent ROS levels in the cells was observed. As a result, induction of ROS may contribute to the cytotoxicity of the amine complex **5a**, which agrees with the results obtained by our previously reported imine complexes.[31−33,52]

2.8. Apoptosis Assay. The pyridyl−imine iridium(III) and ruthenium(II) complexes have been shown to promote cellular death by activating apoptosis in our previous work.[31−33,52] For comparison, the stable pyridyl−amine rhodium(III) complex **5a** was chosen to investigate whether the amine complexes can induce cell apoptosis like imine complexes. A549 cells were incubated with 1, 2, and 3 × IC_{50} of **5a** for 48 h and then analyzed by flow cytometry (Figures 7 and S66). Clearly, treatment with **5a** enhanced the late apoptotic cell populations of the A549 cancer cells compared with the control. Furthermore, concentration-dependent of the proportion of late apoptotic cells was also observed. When **5a** was used at the maximum concentration of 3 × IC_{50}, 92.5% of the treated cells were in late apoptosis. These results indicated that the amine

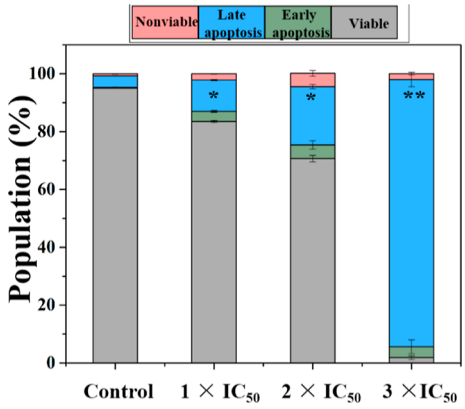

Figure 7. Apoptosis analysis of A549 cells after 48 h of exposure to complex **5a** at 37 °C determined by flow cytometry using AV-fluorescein isothiocyanate versus PI staining. Population of cells in four stages treated with complex **5a**. Data are quoted as mean ± SD of three replicates. *p*-values were calculated after a *t* test against the negative control data; $^{*}p < 0.05$ and $^{**}p < 0.01$.

complex **5a** can arouse the death of cancer cells by inducing apoptosis, which was similar with our previously reported imine iridium(III) complexes.[31,52]

3. CONCLUSIONS

In conclusion, with an easy access to the required pyridine−amine ligands, a series of pyridyl−imine (**2a−2c**, **6**, and **3b−3c**), pyridyl−amine (**4a−4c** and **5a−5c**), and 16-electron pyridyl−amido (7) iridium(III) and rhodium(III) complexes were synthesized and fully characterized. The coordination of these pyridine−amine [N, NH] ligands activated their oxidation to pyridyl−imine [N, N] complexes when molecular oxygen was not totally eliminated. The detection of hydrogen peroxide supported the oxidation mechanism. However, the oxidation of pyridyl−amine complexes to pyridyl−imine complexes was strongly dependent not only on the metal variation and ligand substitution but also on the reaction time and solvents. For example, in the presence of adventitious oxygen, the pyridyl−amine rhodium(III) complex **5a** can be obtained without the formation of the oxidized pyridyl−imine complex, and the pyridyl−amine complex **4b** was cleanly synthesized in the nonpolar solvent CH_2Cl_2. Notably, the oxidation complex **6** with $[(\eta^5\text{-Cp}^*)IrCl_3]$ anions was also synthesized without the addition of the anion exchange reagent NH_4PF_6. The introduction of the bulky *i*-Bu group on the bridge carbon of pyridine−amine ligands afforded the stable 16-electron pyridyl-amido complexes, even when the β hydrogen atom was not excluded and the deprotonating agents were not added. These compounds may represent one of the rarely reported 16-electron coordination mode of half-sandwich complexes. The corresponding pyridyl−amine complexes **4a−4c** and **5a−5c** were also readily prepared under a N_2 atmosphere. The aqueous solution stability study showed that the pyridyl−imine iridium(III) and rhodium(III) complexes underwent hydrolysis, which was consistent with our previous observation of the pyridyl−imine iridium(III) analogues. The instability of pyridyl−amine complexes in aqueous solution could be associated with the formation of the oxidized pyridyl−imine complexes. However, **5a** was stable due to its resistance to oxidation reaction. Most of the complexes in this system showed potent cytotoxicity comparable to that of cisplatin. Particularly, the stable amine complex **5a** displayed the similar IC_{50} value in comparison with

https://doi.org/10.1021/acs.inorgchem.2c00984
Inorg. Chem. 2022, 61, 10051−10065

the imine rhodium(III) complex. The MoA study showed that **5a** exerted its anticancer efficacy by increasing the intracellular ROS level and inducing cell apoptosis.

4. EXPERIMENTAL SECTION

4.1. General Information. All solvents and reagents were purchased from commercial sources. These solvents and reagents were used without further purification unless otherwise claimed. The synthetic routes for ligands **1a−1d** are shown in Supporting Information. The NMR spectroscopy and absorption spectroscopy were performed using Bruker DPX 500 spectrometers and TU-1901 UV−vis recording spectrophotometers, respectively. Mass spectra of the rhodium(III) complexes and iridium(III) complexes were obtained on a Thermo LTQ Orbitrap XL (ESI^+) system. X-ray diffraction data were determined using a Bruker Apex SMART CCD area detector (Tables S1−S7) using graphite-monochromated Mo Kα radiation. C, H, and N elemental analysis was investigated using a Vario EL cube (Figures S54−S57).

4.2. Synthesis of Pyridyl−Imine iridium(III) and rhodium(III) Complexes. General method: $[(\eta^5\text{-Cp}^*)MCl_2]_2$ (M = Ir/Rh) precursors and amine ligands **1a−1c** (2 equiv) were stirred in methanol for 24 h with NH_4PF_6 (2 equiv) at room temperature. Methanol was removed under reduced pressure. The residue was dissolved in dichloromethane and then filtered through Celite. A large amount of *n*-hexane was added to the filtrate, and the product was precipitated, followed by washing with *n*-hexane and diethyl ether and drying under vacuum.

4.2.1. 2a.

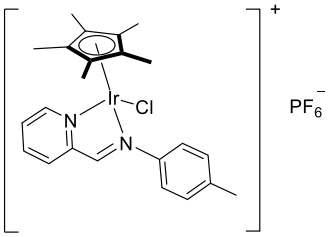

Yield: 53.8 mg (78.0%). ^{1}H NMR (500 MHz, DMSO-d_6): δ 9.34 (s, 1H, C*H*═N), 9.05 (d, J = 5.3 Hz, 1H), 8.41 (d, J = 7.6 Hz, 1H), 8.34 (m, 1H), 7.94 (m, 1H), 7.57 (d, J = 8.3 Hz, 2H), 7.44 (d, J = 8.2 Hz, 2H), 2.43 (s, 3H, aryl-CH_3), 1.43 (s, 15H, Cp*−CH_3). ^{13}C NMR (101 MHz, DMSO-d_6): δ 168.51 (*C*H═N), 155.40, 152.25, 146.41, 146.37, 140.59, 140.54, 139.48, 130.39, 129.78, 129.75, 122.40, 89.69 (C_5Me_5), 20.73 (aryl-*C*H_3), 7.97 (Cp*−*C*H_3). ESI-MS (m/z): calcd for $C_{23}H_{27}ClIrN_2$, 559.1492; , 559.1715 $[M - PF_6]^+$. Anal. Calcd for $C_{23}H_{27}ClF_6IrN_2P$: C, 39.23; H, 3.87; N, 3.98. Found: C, 39.21; H, 3.90; N, 3.95.

4.2.2. 2b.

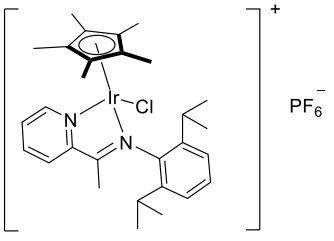

Yield: 51.0 mg (64.0%). ^{1}H NMR (500 MHz, $CDCl_3$): δ 8.91 (d, J = 5.5 Hz, 1H), 8.18 (d, J = 4.0 Hz, 2H), 7.97−7.94 (m, 1H), 7.43−7.31 (m, 3H), 3.62−3.54 (m, 1H, C*H*(CH$_3$)$_2$), 2.61−2.52 (m, 1H, C*H*(CH$_3$)$_2$), 2.43 (s, 3H, C−CH_3), 1.47 (s, 15H, Cp*−CH_3), 1.39 (d, J = 6.6 Hz, 3H, CH(CH_3)$_2$), 1.24 (d, J = 6.6 Hz, 3H, CH(CH_3)$_2$), 1.05−1.01 (m, 6H, CH(CH_3)$_2$). ^{13}C NMR (126 MHz, DMSO-d_6): δ 180.01 (*C*═N), 156.17, 152.24, 142.14, 141.46, 140.45, 140.38, 130.49, 129.07, 128.99, 125.23, 124.52, 90.82 (C_5Me_5), 27.06 (CH(CH$_3$)$_2$), 26.81 (CH-(CH$_3$)$_2$), 25.11 (CH(CH$_3$)$_2$), 24.73 (CH(CH$_3$)$_2$), 24.66 (CH(CH$_3$)$_2$), 23.63 (CH(CH$_3$)$_2$), 21.79 (C−CH$_3$), 8.23 (Cp*−CH$_3$). ESI-MS (m/z): calcd for $C_{29}H_{39}ClIrN_2$, 643.2431; found, 643.2461 $[M - PF_6]^+$. Anal. Calcd for $C_{29}H_{39}ClF_6IrN_2P$: C, 44.19; H, 4.99; N, 3.55. Found: C, 44.03; H, 4.97; N, 3.60.

4.2.3. 2c.

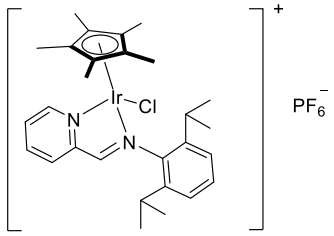

Yield: 55.3 mg (71.5%). ^{1}H NMR (500 MHz, DMSO-d_6): δ 9.64 (s, 1H, C*H*═N), 9.08 (d, J = 5.5 Hz, 1H), 8.47 (d, J = 7.0 Hz, 1H), 8.38−8.35 (m, 1H), 8.03−7.97 (m, 1H), 7.50−7.43 (m, 2H), 7.41−7.39 (m, 1H), 3.86−3.78 (m, 1H, C*H*(CH$_3$)$_2$), 2.47−2.39 (m, 1H, C*H*(CH$_3$)$_2$), 1.45 (s, 15H, Cp*−CH_3), 1.31 (d, J = 6.7 Hz, 3H, CH(CH_3)$_2$), 1.26 (d, J = 6.7 Hz, 3H, CH(CH_3)$_2$), 1.14 (d, J = 6.6 Hz, 3H, CH(CH_3)$_2$), 0.89 (d, J = 6.6 Hz, 3H, CH(CH_3)$_2$). ^{13}C NMR (151 MHz, DMSO-d_6): δ 175.14 (*C*H═N), 155.45, 153.14, 144.65, 142.10, 142.36, 141.41, 131.38, 130.45, 129.77, 124.92, 124.46, 91.24 (C_5Me_5), 27.72 (CH(CH$_3$)$_2$), 27.63 (CH(CH$_3$)$_2$), 27.44 (CH(CH$_3$)$_2$), 26.30 (CH(CH$_3$)$_2$), 24.06 (CH(CH$_3$)$_2$), 21.82 (CH(CH$_3$)$_2$), 8.61 (Cp*−CH$_3$). ESI-MS (m/z): calcd for $C_{28}H_{37}ClIrN_2$, 629.2275; found, 629.2429 $[M - PF_6]^+$. Anal. Calcd for $C_{28}H_{37}ClF_6IrN_2P$: C, 43.44; H, 4.82; N, 3.62. Found: C, 43.47; H, 4.85; N, 3.60.

4.2.4. 3b.

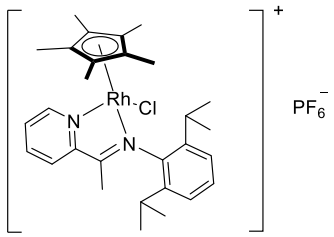

Yield: 50.6 mg (71.2%). ^{1}H NMR (500 MHz, $CDCl_3$): δ 8.93 (d, J = 5.3 Hz, 1H), 8.19−8.16 (m, 1H), 8.08 (d, J = 7.7 Hz, 1H), 7.98−7.92 (m, 1H), 7.43−7.34 (m, 3H), 3.69−3.60 (m, 1H, C*H*(CH$_3$)$_2$), 2.71−2.63 (m, 1H, C*H*(CH$_3$)$_2$), 2.39 (s, 3H, C−CH_3), 1.50 (s, 15H, Cp*−CH_3), 1.41 (d, J = 6.6 Hz, 3H, CH(CH_3)$_2$), 1.27 (d, J = 6.7 Hz, 3H, CH(CH_3)$_2$), 1.04−1.00 (m, 6H, CH(CH_3)$_2$). ^{13}C NMR (151 MHz, DMSO-d_6): δ 178.44 (*C*═N), 154.65, 152.98, 142.60, 141.71, 140.86, 140.69, 130.27, 129.04, 128.98, 125.72, 125.02, 98.23 (C_5Me_5), 27.06 (CH(CH$_3$)$_2$), 27.85 (CH(CH$_3$)$_2$), 27.46 (CH(CH$_3$)$_2$), 25.66 (CH(CH$_3$)$_2$), 25.20 (CH(CH$_3$)$_2$), 24.25 (CH(CH$_3$)$_2$), 22.40 (C−CH$_3$), 8.99 (Cp*−CH$_3$). ESI-MS (m/z): calcd for $C_{29}H_{39}ClRhN_2$, 553.1857; found, 553.1884 $[M - PF_6]^+$. Anal. Calcd for $C_{29}H_{39}ClF_6RhN_2P$: C, 49.83; H, 5.62; N, 4.01. Found: C, 49.85; H, 5.63; N, 4.04.

https://doi.org/10.1021/acs.inorgchem.2c00984
Inorg. Chem. 2022, 61, 10051−10065

4.2.5. 3c.

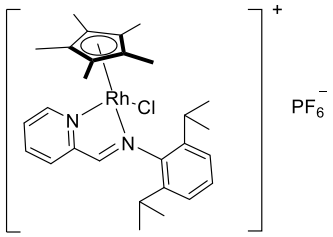

Yield: 46.0 mg (66.7%). ^{1}H NMR (500 MHz, $CDCl_3$): δ 8.89 (d, J = 5.3 Hz, 1H, C*H*═N), 8.38 (d, J = 2.2 Hz, 1H), 8.17 (t, J = 7.7 Hz, 1H), 7.97−7.94 (m, 2H), 7.45−7.38 (m, 2H), 7.33 (d, J = 6.7 Hz, 1H), 3.97−3.89 (m, 1H, C*H*(CH_3)$_2$), 2.72−2.64 (m, 1H, C*H*(CH_3)$_2$), 1.54 (s, 15H, Cp*−CH_3), 1.40 (d, J = 6.6 Hz, 3H, CH(C*H*$_3$)$_2$), 1.34 (d, J = 6.7 Hz, 3H, CH(C*H*$_3$)$_2$), 1.22 (d, J = 6.6 Hz, 3H, CH(C*H*$_3$)$_2$), 0.91 (d, J = 6.6 Hz, 3H, CH(C*H*$_3$)$_2$). ^{13}C NMR (151 MHz, DMSO-d_6): δ 173.09 (*C*H═N), 153.47, 153.24, 144.58, 142.27, 141.76, 141.07, 130.74, 130.47, 129.35, 125.06, 124.36, 98.04 (C_5Me_5), 27.88 (*C*H(CH_3)$_2$), 27.72 (CH(*C*H$_3$)$_2$), 27.57 (CH(*C*H$_3$)$_2$), 26.15 (*C*H(CH_3)$_2$), 24.10 (CH(*C*H$_3$)$_2$), 21.84 (CH(*C*H$_3$)$_2$), 8.88 (Cp*−*C*H$_3$). ESI-MS (m/z): calcd for $C_{28}H_{37}ClRhN_2$, 539.1700; found, 539.1900 [M − PF_6]$^+$. Anal. Calcd for $C_{28}H_{37}ClF_6RhN_2P$: C, 49.10; H, 5.45; N, 4.09. Found: C, 49.08; H, 5.43; N, 4.11.

4.3. Synthesis of Pyridyl−Amine iridium(III) and rhodium(III) Complexes. Method 1 (methanol as solvent): Under a nitrogen atmosphere, [(η^5-Cp*)MCl_2]$_2$ (M = Ir/Rh) precursors and amine ligands **1a−1c** (2 equiv) were stirred in methanol for 2 h with NH_4PF_6 (2 equiv) at room temperature. Methanol was removed under reduced pressure. The residue was dissolved in dichloromethane and then filtered through Celite. A large amount of *n*-hexane was added to the filtrate, and the product was precipitated, followed by washing with *n*-hexane and diethyl ether and drying under vacuum.

Method 2 (dichloromethane as solvent): Under a nitrogen atmosphere, [(η^5-Cp*)MCl_2]$_2$ (M = Ir/Rh) precursors and amine ligands **1a−1c** (2 equiv) were stirred in dichloromethane for 2 h at room temperature. The solvent was removed under reduced pressure. The residue was dissolved in a small amount of ethanol, and then the solution was treated with NH_4PF_6 (2 equiv) and plenty of water. The product was precipitated, followed by washing with *n*-hexane and diethyl ether and drying under vacuum.

4.3.1. 4a.

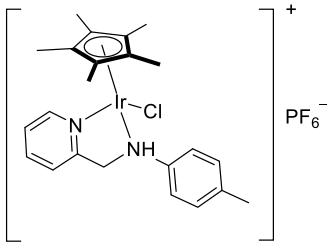

Method 1, yield: 44.0 mg (63.5%). ^{1}H NMR (500 MHz, DMSO-d_6) two isomers. Major isomer/minor isomer = 3:1 (molar ratio). Major isomer: δ 8.73 (d, J = 4.2 Hz, 1H), 8.38 (d, J = 8.8 Hz, 1H), 8.17−8.13 (m, 1H), 7.94 (d, J = 6.9 Hz, 1H), 7.69−7.63 (m, 2H), 7.34−7.33 (m, 3H, aryl-*H* (2H) + N*H* (1H)), 5.04−4.95 (m, 1H, CH_2), 4.60 (d, m, 1H, CH_2), 2.37 (s, 3H, aryl-CH_3), 1.28 (s, 15H, Cp*−CH_3). Minor isomer: δ 9.02 (d, J = 8.3 Hz, 1H), 8.81 (d, J = 4.5 Hz, 1H), 8.22−8.18 (m, 1H), 7.84 (d, J = 7.7 Hz, 1H), 7.41−7.35 (m, 3H), 7.32 (s, 1H), 7.30 (m, 1H, N*H*), 4.86−4.81 (m, 1H, CH_2), 4.60 (d, 1H, CH_2), 2.36 (s, 3H, aryl-CH_3), 1.43 (s, 15H, Cp*−CH_3). ^{13}C NMR (101 MHz, DMSO-d_6) major isomer: δ 159.58, 151.65, 143.48, 143.45, 139.89, 139.87, 135.37, 129.44, 125.41, 122.33, 119.72, 87.28 (C_5Me_5), 58.30 (CH_2), 20.32 (aryl-CH_3), 7.64 (Cp*−CH_3). Minor isomer: δ 159.30, 151.83, 143.63, 143.16, 140.06, 139.45, 135.14, 129.14, 125.99, 122.01, 119.26, 87.04 (C_5Me_5), 58.26 (CH_2), 20.38 (aryl-CH_3), 7.80 (Cp*−CH_3). ESI-MS (m/z): calcd for $C_{23}H_{29}ClIrN_2$, 561.1649; found, 561.1486 [M − PF_6]$^+$. Anal. Calcd for $C_{23}H_{29}ClF_6IrN_2P$: C, 39.12; H, 4.14; N, 3.97. Found: C, 39.15; H, 4.12; N, 3.98.

4.3.2. 4b.

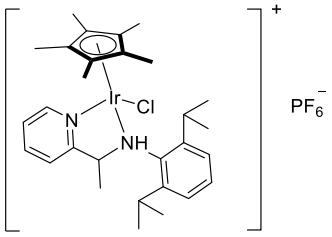

Method 2, yield: 54.8 mg (70.8%). ^{1}H NMR (500 MHz, $CDCl_3$) two isomers. Major isomer/minor isomer = 2:1 (molar ratio). Major isomer: δ 9.09 (d, J = 4.7 Hz, 1H), 8.07−8.04 (m, 1H), 7.85−7.78 (m, 1H), 7.68 (d, J = 7.7 Hz, 1H), 7.25−7.26 (m, 1H), 7.24 (s, 2H), 7.23−7.16 (m, 1H, N*H*), 3.40−3.37 (m, 1H, C*H*(CH_3)$_2$), 2.95−2.87 (m, 1H, C*H*(CH_3)$_2$), 1.62 (s, 15H, Cp*−CH_3), 1.35 (d, J = 5.9 Hz, 6H, CH(C*H*$_3$)$_2$ (3H) + CH−C*H*$_3$ (3H)), 1.28 (d, J = 5.3 Hz, 3H, CH(C*H*$_3$)$_2$), 1.23 (d, J = 6.0 Hz, 3H, CH(C*H*$_3$)$_2$), 1.10 (d, J = 5.8 Hz, 3H, CH(C*H*$_3$)$_2$). Minor isomer: δ 8.70 (d, J = 4.6 Hz, 1H), 8.03−8.00 (m, 1H), 7.64 (m, 1H), 7.47 (d, J = 6.5 Hz, 1H), 7.36 (d, J = 6.6 Hz, 1H), 7.31 (m, 2H), 6.86 (m, 1H, N*H*), 5.26 (m, 1H, C*H*−CH$_3$), 3.33−3.29 (m, 1H, C*H*(CH_3)$_2$), 2.75−2.68 (m, 1H, C*H*(CH_3)$_2$), 1.75 (d, J = 6.3 Hz, 3H, CH−C*H*$_3$), 1.45−1.42 (d, 3H, CH(C*H*$_3$)$_2$), 1.41 (s, 15H, Cp*−CH_3), 1.40−1.39 (m, 3H, CH(C*H*$_3$)$_2$), 1.40−1.38 (m, 6H, CH(C*H*$_3$)$_2$). ^{13}C NMR (151 MHz, DMSO-d_6) major isomer: δ 180.48, 156.68, 152.68, 147.90, 142.72, 141.97, 140.97, 129.52, 125.73, 124.21, 100.96, 91.35 (C_5Me_5), 61.09 (*C*H−CH$_3$), 27.58 (*C*H(CH_3)$_2$), 25.59 (CH(*C*H$_3$)$_2$), 25.22 (*C*H(CH_3)$_2$), 24.71 (CH(*C*H$_3$)$_2$), 24.55 (CH(*C*H$_3$)$_2$), 24.11 (CH(*C*H$_3$)$_2$), 22.28 (CH−*C*H$_3$), 8.74 (Cp*−*C*H$_3$). Minor isomer: δ 180.36, 156.64, 153.04, 147.75, 143.57, 142.62, 140.89, 130.98, 125.81, 125.03, 100.32, 92.65 (C_5Me_5), 60.95 (*C*H−CH$_3$), 27.31 (*C*H(CH_3)$_2$), 25.46 (CH-(*C*H$_3$)$_2$), 25.14 (*C*H(CH_3)$_2$), 24.67 (CH(*C*H$_3$)$_2$), 24.20 (CH(*C*H$_3$)$_2$), 23.89 (*C*H(CH_3)$_2$), 21.53 (CH−*C*H$_3$), 9.13 (Cp*−*C*H$_3$). ESI-MS (m/z): calcd for $C_{29}H_{41}ClIrN_2$, 645.2588; found, 645.2537 [M − PF_6]$^+$. Anal. Calcd for $C_{29}H_{41}ClF_6IrN_2P$: C, 44.07; H, 5.23; N, 3.54. Found: C, 44.03; H, 5.27; N, 3.55.

4.3.3. 4c.

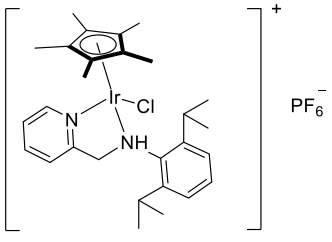

Method 2, yield: 49.1 mg (63.6%). ^{1}H NMR (500 MHz, $CDCl_3$) two isomers. Major isomer/minor isomer = 2:1 (molar ratio). Major isomer: δ 8.92 (d, J = 5.6 Hz, 1H), 8.03−7.99 (m, 1H), 7.80−7.76 (m, 1H), 7.56 (d, J = 7.7 Hz, 1H), 7.38 (d, J = 9.5 Hz, 1H), 7.30 (d, J = 4.6 Hz, 2H), 7.27 (m, 1H, N*H*), 5.18 (m, 1H,

https://doi.org/10.1021/acs.inorgchem.2c00984
Inorg. Chem. 2022, 61, 10051−10065

CH_2), 4.39 (d, 1H, CH_2), 3.15−3.05 (m, 1H, $CH(CH_3)_2$), 2.08−1.99 (m, 1H, $CH(CH_3)_2$), 1.51 (d, J = 6.3 Hz, 3H, $CH(CH_3)_2$), 1.38 (s, 15H, Cp*−CH_3), 1.29 (d, J = 6.8 Hz, 3H, $CH(CH_3)_2$), 1.18 (d, J = 6.5 Hz, 3H, $CH(CH_3)_2$), 1.03 (d, J = 6.5 Hz, 3H, $CH(CH_3)_2$). Minor isomer: δ 9.10 (d, J = 5.7 Hz, 1H), 8.03−7.99 (m, 1H), 7.80−7.76 (m, 2H), 7.25−7.23 (m, 4H, aryl-H (3H) + NH (1H)), 3.64 (s, 2H, CH_2), 3.24−3.15 (m, 2H, $CH(CH_3)_2$), 1.61 (s, 15H, Cp*−CH_3), 1.37−1.36 (d, 6H, $CH(CH_3)_2$), 1.14 (d, J = 6.7 Hz, 6H, $CH(CH_3)_2$). ^{13}C NMR (101 MHz, DMSO-d_6) major isomer: δ 165.27, 151.92, 149.94, 143.26, 139.49, 127.58, 125.67, 124.94, 124.48, 123.94, 121.80, 89.29 (C_5Me_5), 75.62 (CH_2), 27.79 ($CH(CH_3)_2$), 26.72 ($CH(CH_3)_2$), 24.77 ($CH(CH_3)_2$), 9.10(Cp*−CH_3). Minor isomer: δ 164.69, 153.07, 149.16, 145.35, 139.86, 128.31, 126.10, 125.07, 124.19, 123.43, 121.47, 92.65 (C_5Me_5), 54.53 (CH_2), 27.79 ($CH(CH_3)_2$), 27.59 ($CH(CH_3)_2$), 24.47 (CH-$(CH_3)_2$), 8.74(Cp*−CH_3). ESI-MS (m/z): calcd for $C_{28}H_{39}ClIrN_2$, 631.2431; found, 631.2388 $[M - PF_6]^+$. Anal. Calcd for $C_{28}H_{39}ClF_6IrN_2P$: C, 43.32; H, 5.06; N, 3.61. Found: C, 43.34; H, 5.03; N, 3.60.

4.3.4. 5a.

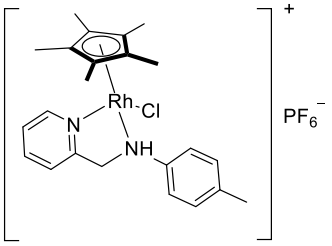

Method 1, yield: 39.0 mg (64.7%). ^{1}H NMR (500 MHz, DMSO-d_6) two isomers. Major isomer/minor isomer = 2:1 (molar ratio). Major isomer: δ 8.73 (d, J = 3.5 Hz, 1H), 8.42−8.27 (m, 1H), 8.13 (d, J = 8.2 Hz, 1H), 7.81 (d, J = 8.2 Hz, 1H), 7.74−7.65 (m, 2H), 7.51−7.42 (m, 1H), 7.33 (m, 2H, aryl-H (1H) + NH (1H)), 4.99−4.91 (m, 1H, CH_2), 4.37−4.29 (m, 1H, CH_2), 2.33 (s, 3H, aryl-CH_3), 1.29 (s, 15H, Cp*−CH_3). Minor isomer: δ 8.80 (d, J = 4.7 Hz, 1H), 8.13 (d, J = 8.2 Hz, 1H), 7.63 (d, J = 7.1 Hz, 2H), 7.51−7.42 (m, 1H), 7.28 (m, 4H, aryl-H (3H) + NH (1H)), 4.58−4.52 (m, 1H, CH_2), 4.37−4.29 (m, 1H, CH_2), 2.33 (s, 3H aryl-CH_3), 1.44 (s, 15H, Cp*−CH_3). ^{13}C NMR (151 MHz, DMSO-d_6) major isomer: δ 159.45, 152.42, 143.66, 140.26, 140.21, 135.35, 130.11, 126.59, 123.17, 122.48, 120.05, 96.08 (C_5Me_5), 57.22 (CH_2), 20.92 (aryl-CH_3), 8.40(Cp*−CH_3). Minor isomer: δ 159.55, 150.84, 144.35, 137.09, 137.04, 136.63, 130.19, 129.84, 126.47, 122.72, 122.44, 95.85 (C_5Me_5), 60.70 (CH_2), 21.06 (aryl-CH_3), 8.60 (Cp*−CH_3). ESI-MS (m/z): calcd for $C_{23}H_{29}ClRhN_2$, 471.1074; found, 471.0000 $[M - PF_6]^+$. Anal. Calcd for $C_{23}H_{29}ClF_6RhN_2P$: C, 44.79; H, 4.74; N, 4.54. Found: C, 44.81; H, 4.77; N, 4.52.

4.3.5. 5b.

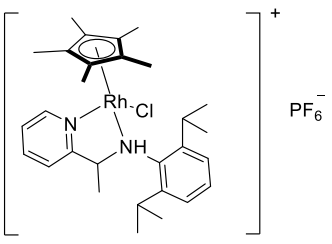

Method 1, yield: 41.6 mg (60.3%). ^{1}H NMR (500 MHz, $CDCl_3$) two isomers. Major isomer/minor isomer = 1:1 (molar ratio). Major isomer: δ 8.73 (d, J = 5.3 Hz, 1H), 7.99 (t, J = 7.3 Hz, 1H), 7.38−7.27 (m, 4H), 7.08−6.93 (m, 1H), 6.51 (d, J = 5.0 Hz, 1H, NH), 5.04−4.96 (m, 1H, CH−CH_3), 3.43−3.36 (m, 1H, $CH(CH_3)_2$), 2.70−2.61 (m, 1H, $CH(CH_3)_2$), 1.65 (d, J = 6.9 Hz, 3H, CH−CH_3), 1.51 (d, J = 10.0 Hz, 6H, $CH(CH_3)_2$), 1.45 (s, 15H, Cp*−CH_3), 1.27 (m, 6H, $CH(CH_3)_2$). Minor isomer: δ 8.63 (d, J = 4.1 Hz, 1H), 7.71−7.64 (m, 1H), 7.53 (t, J = 8.2 Hz, 1H), 7.38−7.27 (m, 1H), 7.16−7.13 (m, 1H), 7.08−6.93 (m, 3H, aryl-H (2H) + NH (1H)), 4.20−4.16 (m, 1H, CH−CH_3), 3.26−3.15 (m, 2H, $CH(CH_3)_2$), 1.45 (s, 15H, Cp*−CH_3), 1.39 (d, J = 6.4 Hz, 3H, CH−CH_3), 1.22 (d, J = 6.8 Hz, 6H, $CH(CH_3)_2$), 1.05 (d, J = 6.8 Hz, 6H, $CH(CH_3)_2$). ^{13}C NMR (101 MHz, DMSO-d_6) major isomer: δ 172.38, 167.27, 163.39, 149.21, 142.02, 141.86, 136.82, 131.91, 128.90, 123.47, 121.76, 99.14 (C_5Me_5), 60.90 (CH−CH_3), 42.34 ($CH(CH_3)_2$), 30.23 ($CH(CH_3)_2$), 27.18 ($CH(CH_3)_2$), 24.27 ($CH(CH_3)_2$), 21.28 ($CH(CH_3)_2$), 18.89 ($CH(CH_3)_2$), 13.78 (CH−CH_3), 8.82 (Cp*−CH_3). Minor isomer: δ 172.30, 166.32, 161.10, 147.79, 141.94, 141.79, 135.99, 131.79, 129.90, 123.17, 122.50, 99.07 (C_5Me_5), 65.31 (CH−CH_3), 44.66 ($CH(CH_3)_2$), 31.51 ($CH(CH_3)_2$), 30.93 ($CH(CH_3)_2$), 29.04 ($CH(CH_3)_2$), 22.33 ($CH(CH_3)_2$), 22.18 ($CH(CH_3)_2$), 14.19 (CH−CH_3), 8.71 (Cp*−CH_3). ESI-MS (m/z): calcd for $C_{29}H_{42}ClF_6RhN_2P$, 701.1739; found, 701.3000 $[M + H]^+$. Anal. Calcd for $C_{29}H_{41}ClF_6RhN_2P$: C, 49.69; H, 5.90; N, 4.00. Found: C, 49.71; H, 5.87; N, 4.02.

4.3.6. 5c.

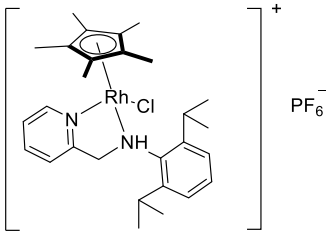

Method 1, yield: 41.8 mg (61.9%). Many of the NMR resonances corresponding to the minor isomer are obscured by those from the major isomer and are therefore not reported. ^{1}H NMR (500 MHz, $CDCl_3$) major isomer: δ 8.93 (d, J = 5.5 Hz, 1H), 7.97 (td, J = 7.7, 1.2 Hz, 1H), 7.79 (t, J = 6.5 Hz, 1H), 7.35 (d, J = 7.8 Hz, 1H), 7.31−7.28 (m, 3H), 7.11−7.08 (m, 1H, NH), 5.00−4.95 (m, 1H, CH_2), 4.14 (d, 1H, CH_2), 3.23−3.13 (m, 1H, $CH(CH_3)_2$), 2.12−2.04 (m, 1H, $CH(CH_3)_2$), 1.51 (d, J = 6.3 Hz, 3H, $CH(CH_3)_2$), 1.43 (s, 15H, Cp*−CH_3), 1.25 (d, J = 6.7 Hz, 3H, $CH(CH_3)_2$), 1.21 (d, J = 6.6 Hz, 3H, $CH(CH_3)_2$), 1.00 (d, J = 6.5 Hz, 3H, $CH(CH_3)_2$). ^{13}C NMR (151 MHz, DMSO-d_6) major isomer: δ 156.75, 146.35, 144.57, 143.18, 142.32, 142.26, 141.75, 125.59, 125.06, 124.46, 124.32, 99.35 (C_5Me_5), 55.41 (CH_2), 27.57 ($CH(CH_3)_2$), 24.77 (CH-$(CH_3)_2$), 9.10 (Cp*−CH_3). ESI-MS (m/z): calcd for $C_{28}H_{39}RhN_2$, 506.2; found, 506.1 $[M - Cl-PF_6]^+$. Anal. Calcd for $C_{28}H_{39}ClF_6RhN_2P$: C, 48.96; H, 5.72; N, 4.08. Found: C, 48.93; H, 5.69; N, 4.11.

4.4. Synthesis of Complexes with [(η^5-Cp*)IrCl$_3$] Anions. The $[(\eta^5\text{-Cp*})IrCl_2]_2$ precursor and amine ligand **1b** (2 equiv) were stirred in methanol for 24 h at room temperature. Methanol was removed under reduced pressure. The residue was dissolved in dichloromethane, and then, a large amount of *n*-hexane was added to the filtrate, and the product was precipitated, followed by washing with *n*-hexane and diethyl ether and drying under vacuum.

https://doi.org/10.1021/acs.inorgchem.2c00984
Inorg. Chem. 2022, 61, 10051−10065

4.4.1. 6.

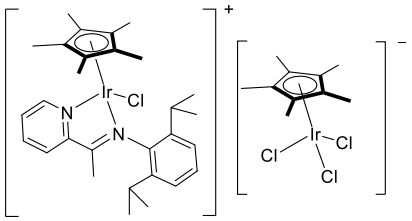

Yield: 35.0 mg (65.7%). ^{1}H NMR (500 MHz, $CDCl_3$): δ 9.18 (d, J = 4.3 Hz, 1H), 8.54−8.45 (m, 2H), 8.40−8.34 (m, 1H), 7.40−7.36 (m, 2H), 7.34−7.31 (m, 1H), 3.62−3.54 (m, 1H, $CH(CH_3)_2$), 2.50 (s, 3H, C−CH_3), 2.47−2.45 (m, 1H, $CH(CH_3)_2$), 1.61 (s, 15H, Cp*−CH_3), 1.50 (s, 15H, Cp*−CH_3), 1.38 (d, J = 6.6 Hz, 3H, $CH(CH_3)_2$), 1.23 (d, J = 6.6 Hz, 3H, $CH(CH_3)_2$), 1.04 (d, J = 6.7 Hz, 3H, $CH(CH_3)_2$), 1.01 (d, J = 6.6 Hz, 3H, $CH(CH_3)_2$). ^{13}C NMR (101 MHz, DMSO-d_6): δ 179.97 (C═N), 156.10, 152.23, 142.08, 141.41, 140.40, 140.31, 130.46, 129.05, 128.93, 125.19, 124.46, 92.04 (C_5Me_5), 90.77 (C_5Me_5), 27.01 ($CH(CH_3)_2$), 26.76 ($CH(CH_3)_2$), 25.08 ($CH(CH_3)_2$), 24.69 ($CH(CH_3)_2$), 24.61 ($CH(CH_3)_2$), 23.59 ($CH(CH_3)_2$), 21.77 (C−CH_3), 8.21 (Cp*−CH_3). ESI-MS (m/z): calcd for $C_{29}H_{39}ClIrN_2$, 643.2431; found, 643.2500 [M − $C_{10}H_{15}Cl_3Ir$]$^+$; ESI-MS (m/z): calcd for $C_{39}H_{53}Cl_4Ir_2N_2$, 1076.2202; found, 1076.2087 [M − H]$^-$. Anal. Calcd for $C_{39}H_{54}Cl_4Ir_2N_2$: C, 43.49; H, 5.05; N, 2.60. Found: C, 43.47; H, 5.02; N, 2.61.

4.5. Synthesis of Pyridyl−Amido Complexes. Complex 7 was synthesized by the reaction of $[(\eta^5\text{-Cp*})IrCl_2]_2$ with **1d** using the same procedure as for the synthesis of pyridyl−imine iridium(III) and rhodium(III) complexes (**2a**−**2c**, **3b**, and **3c**).

4.5.1. 7.

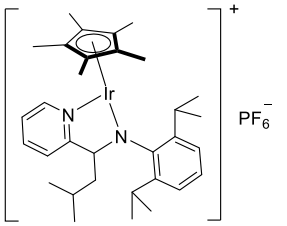

Yield: 55.1 mg (69.8%). ^{1}H NMR (500 MHz, $CDCl_3$): δ 9.10 (d, J = 5.7 Hz, 1H), 8.01 (t, J = 7.7 Hz, 1H), 7.84 (t, J = 6.5 Hz, 1H), 7.64 (d, J = 8.0 Hz, 1H), 7.25 (s, 2H), 7.23−7.19 (m, 1H), 3.42−3.33 (m, 2H, $CH(CH_3)_2$), 2.85−2.75 (m, 1H, $CH(CH_3)_2$), 1.63 (s, 15H, Cp*−CH_3), 1.44 (d, J = 6.8 Hz, 3H, $CH(CH_3)_2$), 1.22 (m, 11H, $CH(CH_3)_2$ (9H) + CH_2 (2H)), 0.83 (d, J = 6.3 Hz, 3H, $CH(CH_3)_2$), 0.76 (d, J = 6.3 Hz, 3H, $CH(CH_3)_2$). ^{13}C NMR (126 MHz, $CDCl_3$): δ 168.24, 151.78, 148.86, 143.76, 143.56, 138.59, 127.23, 126.07, 124.70, 124.33, 121.28, 89.49 (C_5Me_5), 82.48 (CH−N), 43.45 (CH_2), 27.30 ($CH(CH_3)_2$), 26.95 ($CH(CH_3)_2$), 26.78 ($CH(CH_3)_2$), 26.39 ($CH(CH_3)_2$), 26.28 ($CH(CH_3)_2$), 26.20 ($CH(CH_3)_2$), 25.79 ($CH(CH_3)_2$), 23.59 ($CH(CH_3)_2$), 21.05 ($CH(CH_3)_2$), 9.45 (Cp*−CH_3). ESI-MS (m/z): calcd $C_{32}H_{46}IrN_2$ 651.3290; found, 651.3446 [M − PF_6]$^+$. Anal. Calcd for $C_{32}H_{46}F_6IrN_2P$: C, 48.29; H, 5.83; N, 3.52. Found: C, 48.33; H, 5.85; N, 3.60.

■ ASSOCIATED CONTENT

Supporting Information

The Supporting Information is available free of charge at https://pubs.acs.org/doi/10.1021/acs.inorgchem.2c00984.

Details of the experimental section, proposed mechanisms, ^{1}H and ^{13}C NMR spectra, ESI-MS spectra, C,H,and N elemental analysis of the complexes, UV-vis spectra for complexes, time-dependent ^{1}H NMR spectroscopic stability study, apoptosis analysis of A549 cells, bond lengths and angles, and IC50 values (PDF)

Accession Codes

CCDC 2160775, 2160785, 2160944, 2160963, and 2160992−2160994 contain the supplementary crystallographic data for this paper. These data can be obtained free of charge via www.ccdc.cam.ac.uk/data_request/cif, or by emailing data_request@ccdc.cam.ac.uk, or by contacting The Cambridge Crystallographic Data Centre, 12 Union Road, Cambridge CB2 1EZ, UK; fax: +44 1223 336033.

■ AUTHOR INFORMATION

Corresponding Authors

Lihua Guo − *School of Chemistry and Chemical Engineering, Qufu Normal University, Qufu 273165, P. R. China;* orcid.org/0000-0002-0842-9958; Email: guolihua@qfnu.edu.cn

Zhe Liu − *School of Chemistry and Chemical Engineering, Qufu Normal University, Qufu 273165, P. R. China;* orcid.org/0000-0001-5796-4335; Email: liuzheqd@163.com

Authors

Xueyan Hu − *School of Chemistry and Chemical Engineering, Qufu Normal University, Qufu 273165, P. R. China*

Mengqi Liu − *School of Chemistry and Chemical Engineering, Qufu Normal University, Qufu 273165, P. R. China*

Mengru Sun − *School of Chemistry and Chemical Engineering, Qufu Normal University, Qufu 273165, P. R. China*

Qiuya Zhang − *School of Chemistry and Chemical Engineering, Qufu Normal University, Qufu 273165, P. R. China*

Hongwei Peng − *School of Chemistry and Chemical Engineering, Qufu Normal University, Qufu 273165, P. R. China*

Fanjun Zhang − *School of Chemistry and Chemical Engineering, Qufu Normal University, Qufu 273165, P. R. China*

Complete contact information is available at: https://pubs.acs.org/10.1021/acs.inorgchem.2c00984

Notes

The authors declare no competing financial interest.

■ ACKNOWLEDGMENTS

We thank the Young Talents Invitation Program of Shandong Provincial Colleges and Universities, the Taishan Scholars Program, the National Natural Science Foundation of China (grant no. 21901140), and the Key Laboratory of Polymeric Composite & Functional Materials of Ministry of Education (PCFM-2021A01) and Natural Science Foundation of Shandong Province (ZR2019BB078) for support.

■ REFERENCES

(1) Wang, D.; Lippard, S. J. Cellular processing of platinum anticancer drugs. *Discov* **2005**, *4*, 307−320.

(2) Rosenberg, B.; Van Camp, L.; Krigas, T. Inhibition of Cell Division in Escherichia coli by Electrolysis Products from a Platinum Electrode. *Nature* **1965**, *205*, 698−699.

(3) Kelland, L. The resurgence of platinum-based cancer chemotherapy. *Nat. Rev. Cancer* **2007**, *7*, 573−584.

(4) Cepeda, V.; Fuertes, M. A.; Castilla, J.; Alonso, C.; Quevedo, C.; Perez, J. M. Biochemical Mechanisms of Cisplatin Cytotoxicity. *Anti-Cancer Agents Med. Chem.* **2007**, *7*, 3−18.
(5) Giaccone, G.; Herbst, R. S.; Manegold, C.; Scagliotti, G.; Rosell, R.; Miller, V.; Natale, R. B.; Schiller, J. H.; von Pawel, J.; Pluzanska, A.; Gatzemeier, U.; Grous, J.; Ochs, J. S.; Averbuch, S. D.; Wolf, M. K.; Rennie, P.; Fandi, A.; Johnson, D. H. Gefitinib in Combination With Gemcitabine and Cisplatin in Advanced Non-Small-Cell Lung Cancer: A Phase III Trial-INTACT 1. *J. Clin. Oncol.* **2004**, *22*, 777−784.
(6) Li, Y.; Tan, C.-P.; Zhang, W.; He, L.; Ji, L.-N.; Mao, Z.-W. Phosphorescent iridium(III)-bis-N-heterocyclic carbene complexes as mitochondria-targeted theranostic and photodynamic anticancer agents. *Biomaterials* **2015**, *39*, 95−104.
(7) Su, X.; Wang, W.-J.; Cao, Q.; Zhang, H.; Liu, B.; Ling, Y.; Zhou, X.; Mao, Z.-W. A Carbonic Anhydrase IX (CAIX)-Anchored Rhenium(I) Photosensitizer Evokes Pyroptosis for Enhanced Anti-Tumor Immunity. *Angew. Chem., Int. Ed.* **2022**, *61*, No. e202115800.
(8) Gichumbi, J. M.; Friedrich, H. B. Half-sandwich complexes of platinum group metals (Ir, Rh, Ru and Os) and some recent biological and catalytic applications. *J. Organomet. Chem.* **2018**, *866*, 123−143.
(9) Geldmacher, Y.; Oleszak, M.; Sheldrick, W. S. Rhodium(III) and iridium(III) complexes as anticancer agents. *Inorg. Chim. Acta* **2012**, *393*, 84−102.
(10) Hartinger, C. G.; Metzler-Nolte, N.; Dyson, P. J. Challenges and Opportunities in the Development of Organometallic Anticancer Drugs. *Organometallics* **2012**, *31*, 5677−5685.
(11) Konkankit, C. C.; Marker, S. C.; Knopf, K. M.; Wilson, J. J. Anticancer activity of complexes of the third row transition metals, rhenium, osmium, and iridium. *Dalton Trans.* **2018**, *47*, 9934−9974.
(12) Romero-Canelón, I.; Sadler, P. J. Next-Generation Metal Anticancer Complexes: Multitargeting via Redox Modulation. *Inorg. Chem.* **2013**, *52*, 12276−12291.
(13) Leung, C.-H.; Zhong, H.-J.; Chan, D. S.-H.; Ma, D.-L. Bioactive iridium and rhodium complexes as therapeutic agents. *Coord. Chem. Rev.* **2013**, *257*, 1764−1776.
(14) Dorcier, A.; Ang, W. H.; Bolaño, S.; Gonsalvi, L.; Juillerat-Jeannerat, L.; Laurenczy, G.; Peruzzini, M.; Phillips, A. D.; Zanobini, F.; Dyson, P. J. In Vitro Evaluation of Rhodium and Osmium RAPTA Analogues: The Case for Organometallic Anticancer Drugs Not Based on Ruthenium. *Organometallics* **2006**, *25*, 4090−4096.
(15) Almodares, Z.; Lucas, S. J.; Crossley, B. D.; Basri, A. M.; Pask, C. M.; Hebden, A. J.; Phillips, R. M.; McGowan, P. C. Rhodium, Iridium, and Ruthenium Half-Sandwich Picolinamide Complexes as Anticancer Agents. *Inorg. Chem.* **2014**, *53*, 727−736.
(16) Liu, Z.; Sadler, P. J. Organoiridium Complexes: Anticancer Agents and Catalysts. *Acc. Chem. Res.* **2014**, *47*, 1174−1185.
(17) Rono, C. K.; Chu, W. K.; Darkwa, J.; Meyer, D.; Makhubela, B. C. E. Triazolyl Ru^{II}, Rh^{III}, Os^{II}, and Ir^{III} Complexes as Potential Anticancer Agents: Synthesis, Structure Elucidation, Cytotoxicity, and DNA Model Interaction Studies. *Organometallics* **2019**, *38*, 3197−3211.
(18) Mukhopadhyay, S.; Gupta, R. K.; Paitandi, R. P.; Rana, N. K.; Sharma, G.; Koch, B.; Rana, L. K.; Hundal, M. S.; Pandey, D. S. Synthesis, Structure, DNA/Protein Binding, and Anticancer Activity of Some Half-Sandwich Cyclometalated Rh(III) and Ir(III) Complexes. *Organometallics* **2015**, *34*, 4491−4506.
(19) Truong, D.; Sullivan, M. P.; Tong, K. K. H.; Steel, T. R.; Prause, A.; Lovett, J. H.; Andersen, J. W.; Jamieson, S. M. F.; Harris, H. H.; Ott, I.; Weekley, C. M.; Hummitzsch, K.; Söhnel, T.; Hanif, M.; Metzler-Nolte, N.; Goldstone, D. C.; Hartinger, C. G. Potent Inhibition of Thioredoxin Reductase by the Rh Derivatives of Anticancer M(arene/Cp*)(NHC)Cl_2 Complexes. *Inorg. Chem.* **2020**, *59*, 3281−3289.
(20) Gupta, G.; Kumari, P.; Ryu, J. Y.; Lee, J.; Mobin, S. M.; Lee, C. Y. Mitochondrial Localization of Highly Fluorescent and Photostable BODIPY-Based Ruthenium(II), Rhodium(III), and Iridium(III) Metal Complexes. *Inorg. Chem.* **2019**, *58*, 8587−8595.
(21) Petrini, A.; Pettinari, R.; Marchetti, F.; Pettinari, C.; Therrien, B.; Galindo, A.; Scopelliti, R.; Riedel, T.; Dyson, P. J. Cytotoxic Half-Sandwich Rh(III) and Ir(III) β-Diketonates. *Inorg. Chem.* **2017**, *56*, 13600−13612.
(22) Maji, M.; Acharya, S.; Bhattacharya, I.; Gupta, A.; Mukherjee, A. Effect of an Imidazole-Containing Schiff Base of an Aromatic Sulfonamide on the Cytotoxic Efficacy of N,N-Coordinated Half-Sandwich Ruthenium(II) p-Cymene Complexes. *Inorg. Chem.* **2021**, *60*, 4744−4754.
(23) Yang, Y.; Guo, L.; Tian, Z.; Ge, X.; Gong, Y.; Zheng, H.; Shi, S.; Liu, Z. Lysosome-Targeted Phosphine-Imine Half-Sandwich Iridium(III) Anticancer Complexes: Synthesis, Characterization, and Biological Activity. *Organometallics* **2019**, *38*, 1761−1769.
(24) Ludwig, G.; Mijatović, S.; Ranđelović, I.; Bulatović, M.; Miljković, D.; Maksimović-Ivanić, D.; Korb, M.; Lang, H.; Steinborn, D.; Kaluđerović, G. N. Biological activity of neutral and cationic iridium(III) complexes with κP and κP,κS coordinated Ph_2PCH_2S-$(O)_x$Ph (x = 0−2) ligands. *Eur. J. Med. Chem.* **2013**, *69*, 216−222.
(25) Broomfield, L. M.; Alonso-Moreno, C.; Martin, E.; Shafir, A.; Posadas, I.; Ceña, V.; Castro-Osma, J. A. Aminophosphine ligands as a privileged platform for development of antitumoral ruthenium(II) arene complexes. *Dalton Trans.* **2017**, *46*, 16113−16125.
(26) Yang, Y.; Guo, L.; Ge, X.; Shi, S.; Gong, Y.; Xu, Z.; Zheng, X.; Liu, Z. Structure-activity relationships for highly potent half-sandwich organoiridium(III) anticancer complexes with ĈN-chelated ligands. *J. Inorg. Biochem.* **2019**, *191*, 1−7.
(27) Liu, Z.; Habtemariam, A.; Pizarro, A. M.; Fletcher, S. A.; Kisova, A.; Vrana, O.; Salassa, L.; Bruijnincx, P. C. A.; Clarkson, G. J.; Brabec, V.; Sadler, P. J. Organometallic Half-Sandwich Iridium Anticancer Complexes. *J. Med. Chem.* **2011**, *54*, 3011−3026.
(28) Zhang, H.; Guo, L.; Tian, Z.; Tian, M.; Zhang, S.; Xu, Z.; Gong, P.; Zheng, X.; Zhao, J.; Liu, Z. Significant effects of counteranions on the anticancer activity of iridium(III) complexes. *Chem. Commun.* **2018**, *54*, 4421−4424.
(29) Liu, Z.; Romero-Canelón, I.; Qamar, B.; Hearn, J. M.; Habtemariam, A.; Barry, N. P. E.; Pizarro, A. M.; Clarkson, G. J.; Sadler, P. J. The Potent Oxidant Anticancer Activity of Organoiridium Catalysts. *Angew. Chem., Int. Ed.* **2014**, *53*, 3941−3946.
(30) Liu, Z.; Romero-Canelón, I.; Habtemariam, A.; Clarkson, G. J.; Sadler, P. J. Potent Half-Sandwich Iridium(III) Anticancer Complexes Containing C∧N-Chelated and Pyridine Ligands. *Organometallics* **2014**, *33*, 5324−5333.
(31) Li, J.; Guo, L.; Tian, Z.; Tian, M.; Zhang, S.; Xu, K.; Qian, Y.; Liu, Z. Novel half-sandwich iridium(III) imino-pyridyl complexes showing remarkable in vitro anticancer activity. *Dalton Trans.* **2017**, *46*, 15520−15534.
(32) Tian, M.; Li, J.; Zhang, S.; Guo, L.; He, X.; Kong, D.; Zhang, H.; Liu, Z. Half-sandwich ruthenium(II) complexes containing N̂N-chelated imino-pyridyl ligands that are selectively toxic to cancer cells. *Chem. Commun.* **2017**, *53*, 12810−12813.
(33) Tian, Z.; Li, J.; Zhang, S.; Xu, Z.; Yang, Y.; Kong, D.; Zhang, H.; Ge, X.; Zhang, J.; Liu, Z. Lysosome-Targeted Chemotherapeutics: Half-Sandwich Ruthenium(II) Complexes That Are Selectively Toxic to Cancer Cells. *Inorg. Chem.* **2018**, *57*, 10498−10502.
(34) Yang, Y.; Guo, L.; Ge, X.; Zhu, T.; Chen, W.; Zhou, H.; Zhao, L.; Liu, Z. The Fluorine Effect in Zwitterionic Half-Sandwich Iridium(III) Anticancer Complexes. *Inorg. Chem.* **2020**, *59*, 748−758.
(35) Yang, Y.; Ge, X.; Guo, L.; Zhu, T.; Tian, Z.; Zhang, H.; Du, Q.; Peng, H.; Ma, W.; Liu, Z. Zwitterionic and cationic half-sandwich iridium(III) ruthenium(II) complexes bearing sulfonate groups: synthesis, characterization and their different biological activities. *Dalton Trans.* **2019**, *48*, 3193−3197.
(36) Guo, L.; Hu, X.; Yang, Y.; An, W.; Gao, J.; Liu, Q.; Liu, Z. Synthesis and biological evaluation of zwitterionic half-sandwich Rhodium(III) and Ruthenium(II) organometallic complexes. *Bioorg. Chem.* **2021**, *116*, 105311.
(37) Kennedy, D. F.; Messerle, B. A.; Smith, M. K. Synthesis of Cp* Iridium and Rhodium Complexes Containing Bidentate sp^2-N-Donor Ligands and Counter-Anions $[Cp^*MCl_3]^-$. *Eur. J. Inorg. Chem.* **2007**, *2007*, 80−89.
(38) Zain Aldin, M.; Zaragoza, G.; Deschamps, W.; Tomani, J.-C. D.; Souopgui, J.; Delaude, L. Synthesis, Characterization, and Biological Activity of Water-Soluble, Dual Anionic and Cationic Ruthenium-

https://doi.org/10.1021/acs.inorgchem.2c00984
Inorg. Chem. 2022, 61, 10051−10065

Arene Complexes Bearing Imidazol(in)ium-2-dithiocarboxylate Ligands. *Inorg. Chem.* **2021**, *60*, 16769−16781.
(39) Zai, S.; Liu, F.; Gao, H.; Li, C.; Zhou, G.; Cheng, S.; Guo, L.; Zhang, L.; Zhu, F.; Wu, Q. Longstanding living polymerization of ethylene: substituent effect on bridging carbon of 2-pyridinemethanamine nickel catalysts. *Chem. Commun.* **2010**, *46*, 4321−4323.
(40) Crabtree, R. H. *The Organometallic Chemistry of the Transition Metals*, 6th ed.; John Wiley & Sons, 2009; pp 73.
(41) Thangavel, S.; Boopathi, S.; Mahadevaiah, N.; Kolandaivel, P.; Pansuriya, P. B.; Friedrich, H. B. Catalytic oxidation of primary aromatic alcohols using half sandwich Ir(III), Rh(III) and Ru(II) complexes: A practical and theoretical study. *J. Mol. Catal. A: Chem.* **2016**, *423*, 160−171.
(42) Gómez, J.; García-Herbosa, G.; Cuevas, J. V.; Arnáiz, A.; Carbayo, A.; Muñoz, A.; Falvello, L.; Fanwick, P. E. Diastereospecific and Diastereoselective Syntheses of Ruthenium(II) Complexes Using N,N' Bidentate Ligands Aryl-pyridin-2-ylmethyl-amine ArNH-CH_2-2-C_5H_4N and Their Oxidation to Imine Ligands. *Inorg. Chem.* **2006**, *45*, 2483−2493.
(43) Thangavel, S.; Friedrich, H. B.; Omondi, B. Syntheses and structural investigations of new half sandwich Ir(III) and Rh(III) amine compounds and their catalytic transfer hydrogenation of aromatic ketones and aldehydes in water. *Mol. Catal.* **2017**, *429*, 27−42.
(44) Richard Keene, F. Metal-ion promotion of the oxidative dehydrogenation of coordinated amines and alcohols. *Coord. Chem. Rev.* **1999**, *187*, 121−149.
(45) Kuwata, S.; Ikariya, T. *β*-Protic Pyrazole and N-Heterocyclic Carbene Complexes: Synthesis, Properties, and Metal-Ligand Cooperative Bifunctional Catalysis. *Chem.—Eur. J.* **2011**, *17*, 3542−3556.
(46) Han, Y.; Liu, X.; Tian, Z.; Ge, X.; Li, J.; Gao, M.; Li, Y.; Liu, Y.; Liu, Z. Half-sandwich Iridium(III) Benzimidazole-Appended Imidazolium-Based N -heterocyclic Carbene Complexes and Antitumor Application. *Chem.−Asian J.* **2018**, *13*, 3697−3705.
(47) Nagashima, H.; Kondo, H.; Hayashida, T.; Yamaguchi, Y.; Gondo, M.; Masuda, S.; Miyazaki, K.; Matsubara, K.; Kirchner, K. Chemistry of coordinatively unsaturated organoruthenium amidinates as entry to homogeneous catalysis. *Coord. Chem. Rev.* **2003**, *245*, 177−190.
(48) Zamorano, A.; Rendón, N.; López-Serrano, J.; Álvarez, E.; Carmona, E. Activation of Small Molecules by the Metal−Amido Bond of Rhodium(III) and Iridium(III) (η^5-C_5Me_5)M-Aminopyridinate Complexes. *Inorg. Chem.* **2018**, *57*, 150−162.
(49) Li, Z.; Wu, F.-Y.; Guo, L.; Li, A.-F.; Jiang, Y.-B. Enhanced Anion Binding of N-(Anilino)thioureas. Contribution of the N-Anilino −NH Proton Acidity. *J. Phys. Chem. B* **2008**, *112*, 7071−7079.
(50) Petra, D. G. I.; Reek, J. N. H.; Handgraaf, J.-W.; Meijer, E. J.; Dierkes, P.; Kamer, P. C. J.; Brussee, J.; Schoemaker, H. E.; van Leeuwen, P. W. N. M. Chiral Induction Effects in Ruthenium(II) Amino Alcohol Catalysed Asymmetric Transfer Hydrogenation of Ketones: An Experimental and Theoretical Approach. *Chem.—Eur. J.* **2000**, *6*, 2818−2829.
(51) Hohmann, H.; Hellquist, B.; Van Eldik, R. Kinetics and mechanism of the complex formation reactions of diaqua(ethylenediamine)- and diaqua(tetraethylethylenediamine)palladium(II) with the purine nucleosides adenosine and inosine. *Inorg. Chem.* **1992**, *31*, 345−351.
(52) Li, J.; Guo, L.; Tian, Z.; Zhang, S.; Xu, Z.; Han, Y.; Li, R.; Li, Y.; Liu, Z. Half-Sandwich Iridium and Ruthenium Complexes: Effective Tracking in Cells and Anticancer Studies. *Inorg. Chem.* **2018**, *57*, 13552−13563.

https://doi.org/10.1021/acs.inorgchem.2c00984
Inorg. Chem. 2022, 61, 10051−10065